Dynamics of the epigenetic landscape during development and in response to drought stress in sorghum

Yongfeng Hu[1, †, *], Chao He[2, †], Yuning Shen[2], Gongjian Zeng[1], Siteng Bi[2], Quanjun Huang[1], Xiner Qin[1], Zhuying Deng[1], Zhengquan He[1], Xiangling Shen[1,*]

[1]Key Laboratory of Three Gorges Regional Plant Genetics & Germplasm Enhancement (CTGU)/ Biotechnology Research Center, College of Biological and Pharmaceutical Sciences, China Three Gorges University, Yichang, Hubei 443002, China.

[2]National Key Laboratory of Crop Genetic Improvement, Hubei Hongshan Laboratory, Huazhong Agricultural University, Wuhan, China.

[†]These authors contributed equally to this work.

[*]Corresponding author: huyongfeng@ctgu.edu.cn; shenxl1982@hotmail.com

Abstract

Sorghum bicolor is a C4 plant with the characteristics of high stress tolerance, which may be conferred partly by the underlying epigenetic mechanism unique to sorghum. In this study, we revealed some epigenomic features in sorghum that have never been reported before. The long H3K27me3 regions clustered in four areas, which we defined as H3K27me3 islands, were identified in sorghum. H3K36me3 plays some role in inhibiting the deposition of both H3K27me3 and H2A.Z, which may serve as partial motivation for the removal of H3K27me3 and H2A.Z in leaf and root. All the 7 histone marks are involved in the regulation of tissue-specific genes, especially the specific expression of C4 genes in leaf and peroxidase (POD) encoding genes in root, which are involved in the photosynthesis in leaf and lignin synthesis in root, respectively. These marks except H3K36me3 and H3K27me3 also engage in the regulation of stress genes in response to PEG treatment. However, we found that differential enrichment of histone marks on many tissue-specific genes was observed only between leaf and root but hardly in response to PEG treatment, although expression of these genes changed after PEG treatment.

Key words: sorghum, histone modification, H2A.Z, root and leaf, drought stress

Introduction

Histone marks play important roles in gene regulation, and they exhibit different distribution patterns in intragenic regions. Histone acetylation and H3K4me3 tend to mark transcription start site (TSS) regions (a short region immediately downstream from TSS), while H3K36me3 are more likely to be enriched in gene body regions (a longer region from TSS to transcription end site (TES)) (Barski et al. 2007; Guenther et al. 2007; Hu et al. 2020), suggesting that they are involved in governing different processes of gene transcription. Histone acetylation and H3K4me3 have been reported to be involved in transcription initiation by affecting the assembly of pre-initiation complex (PIC), or stimulating the transition from initiation to elongation (Ding et al. 2012; Lauberth et al. 2013; Gates et al. 2017; Wang et al. 2023). H3K36me3, generally considered as a hallmark of transcription elongation, is required for co-transcriptional splicing (Guenther et al. 2007; Iwamori et al. 2016; Sorenson et al. 2016). The distribution patterns of some histone marks are similar in different species while the others are not. For example, in humans and yeast, H3K36me3 is excluded from TSS of genes while there is a clear enrichment peak of the mark around TSS in plants (Barski et al. 2007; Li et al. 2015; Liu et al. 2016; Suzuki et al. 2016). In animals, H3K27me3 can spread to hundreds of kilobases and cover several genes per region (Schwartz et al. 2006). However, most of H3K27me3 regions in *Arabidopsis* are limited to single genes (Zhang et al. 2007). The different distribution patterns of these histone marks may reflect diverse deposition mechanism of them in different species.

The complex crosstalk between different histone modifications is established, since the activity of histone modifiers depositing one histone mark could be either promoted or inhibited by other histone marks. For instance, H2B ubiquitylation is required for simulating the activity of the MLL complex to catalyze H3K4me3 (Hsu et al. 2019). H3K4me3 provides the binding platform for the HAT complexes, facilitating histone acetylations (Taverna et al. 2006; Ringel et al. 2015). The interplay between repressive marks such as H3K27me3 and H2AK119ub1, which are deposited by Polycomb repressive complex 2 (PRC2) and Polycomb repressive complex 1 (PRC1) respectively, have also been unraveled (Blackledge and Klose 2021). Interestingly, both PRC2 and PRC1 can read the two marks to establish or reinforce these modifications (Blackledge and Klose 2021). By contrast, H3K4me3 and H3K36me3

inhibit the activity of PRC2 (Schmitges et al. 2011; Finogenova et al. 2020). Furthermore, it has been demonstrated that H3K36me3 and H3K27me3 are rarely present on the same histone tail in various species (Yuan et al. 2011; Yang et al. 2014), suggesting that the inhibitory effect of H3K36me3 on deposition of H3K27me3 is conserved. Indeed, genome-wide analysis of chromatin states indicates that the distributed regions of some histone marks highly co-exist while the others are seldom overlapped, which is well consistent with the crosstalk between them (Ernst et al. 2011; Sequeira-Mendes et al. 2014).

Sorghum is an ideal model species for analyzing genetic features of C4 plants due to its small genome and natural diploid. Besides, it also exhibits high tolerance to various abiotic stresses, making it a good candidate for studying mechanism of plant stress tolerance. In this paper, genome-wide analysis of various histone modification enrichment was conducted in sorghum root and leave before and after PEG treatment to explore the role of epigenetic marks in the regulation of sorghum development and stress response. We found that distribution pattern of these marks in sorghum was similar to that reported in other plant species. However, sorghum-specific epigenomic features were also revealed.

Results

Distribution pattern analysis of histone marks reveals four H3K27me3 islands in sorghum

Three replicates for RNA-seq and two biological replicates for ChIP-seq in leaf and root of sorghum were performed with antibodies against various histone modifications (H3K9ac, H3K27ac, H3K4me3, H3K36me3, H3K4me2 and H3K27me3) and H2A.Z. The three replicates of RNA-seq analysis were highly correlated (Fig. S1a). For most of the ChIP-seq samples, more than 20 million reads were obtained, the overall mapping rate was more than 85% (Table S1), the FRiP value and the SPOT value were greater than 0.5 (Fig. S1b). The two biological replicates of ChIP-seq were also highly correlated (Fig. S1c). Genome-wide view of histone mark enrichment demonstrate that the distribution of all the 7 histone marks was highly correlated with gene density, which is relatively higher at both ends of each chromosome and lower in the middle of the chromosome (Fig. S2). These results suggest that all the data are reliable for subsequent analysis.

To attempt to investigate the distribution pattern of histone marks, intragenic peaks (located from 1.5 kb upstream from gene TSS to 1.5 kb downstream from gene TES) were called for creating metaplots and heat maps (Fig. 1a and 1b). The results showed that H3K9ac, H3K27ac, H3K4me3 were predominantly enriched in TSS regions. H3K4me2 and H2A.Z were distributed either TSS regions or gene body regions. H3K36me3 enrichment extended from TSS in gene body but not to TES. The distribution patterns of these histone marks are similar to those in *Arabidopsis* and rice (Zilberman et al. 2008; Roudier et al. 2009; Li et al. 2015; Hu et al. 2020). We also found strong H3K27me3 enrichment in gene body in both root and leaf. Interestingly, low H3K27me3 enrichment in TSS regions was observed in leaf but not in root (Fig. 1b), which has never been reported in plants before. Besides, genome-wide enrichment of H3K4me2, H3K36me3, H3K27me3 and H2A.Z was decreased in root, suggesting their possible regulatory roles in the fine-tuning of developmental genes (Fig. 1a).

In animals, H3K27me3 enrichment can spread to more than one hundred kilobases, which usually cover several genes (Schwartz et al. 2006). It seems that in *Arabidopsis* H3K27me3 coverage is confined to single gene (Zhang et al. 2007). To determine whether H3K27me3 in sorghum is distributed similarly, we analyzed length of H3K27me3 regions and number of genes per region. The results showed that most of H3K27me3 regions were short and covered single genes in sorghum (Fig. 1c and 1d), which is similar as in *Arabidopsis*. However, we found considerable long H3K27me3 regions in sorghum (Fig. 1c and 1d). The maximum length can reach more than two hundred kilobases. Three H3K27me3 regions covered more than 20 genes (Fig. 1d). In addition, there were more short regions and less long regions in leaf than those in root, suggesting that H3K27me3 enrichment in the two organs are reprogrammed. When we visualized genome-wide H3K27me3 regions, we found four areas on Chromosomes 2, 5 and 8 where long H3K27me3 regions clustered, which we termed the H3K27me3 islands (Fig. 1e). The other long H3K27me3 regions scattered in the other part of the genome. The similar analysis was performed in *Arabidopsis* and rice by using the recently deposited high quality data (see Material and methods). The long H3K27me3 regions were also identified in *Arabidopsis* and rice despite that the number was less than that in sorghum (Fig. S3a), especially the regions longer than 50kb. In addition, the H3K27me3 island was not observed in *Arabidopsis* and rice (Fig. S3c). However, the genes covered by long H3K27me3

regions were greater in *Arabidopsis* (Fig. S3b), which may be due to the higher gene density. This indicates that plant epigenomes contain both gene-specific and long region of H3K27me3 enrichment.

Antagonistic relationship between H3K36me3 enrichment and H3K27me3 enrichment as well as H2A.Z deposition

To analyze the relationship between different histone marks in sorghum, we clustered distribution patterns of each histone mark in intragenic region (from 0.5kb upstream TSS to 3kb downstream TSS) into three categories (C1, C2 and C3), and observe how the other histone marks are distributed in the same category. We found that H3K9ac, H3K27ac, H3K4me3 enriched in the TSS region and H3K36me3 enriched in the gene body region are highly overlapped and associated with actively transcribed genes (Fig. 2a-2d, S4a-S4d). The gene-body- enriched H3K27me3 is exclusive with the above histone modifications especially H3K36me3, and is associated with silent genes (Fig. 2g, Fig. S4g). The partial overlapping of H3K4me3 and H3K27me3 suggests the existence of the bivalent mark in sorghum. The distributions of H3K4me2 and H2A.Z in different regions displayed distinct relationships with the other marks (Fig. 2e-2f, Fig. S4e-S4f). The strong enrichment of H2A.Z in the gene body region (C1) overlapped with the repressive mark (H3K27me3), whereas the weak enrichment of H2A.Z in the TSS region (C3) overlapped with the active marks (H3K9ac, H3K27ac, H3K36me3) (Fig. 2e, Fig. S4e). By contrast, H3K4me2 deposited in the TSS region (C1) co-existed with the repressive mark, whereas that deposited in the gene body region (C2) co-existed with the active marks (Fig. 2f, Fig. S4f). Furthermore, we found that H3K4me2 and H3K4me3 co-existed in many genes although distribution patterns of the two marks in these genes were slightly different. This suggests that the nucleosome simultaneously carrying H3K4me2 and H3K4me3 is common in sorghum, but the deposition of the two marks may be independent.

Considering the strictly antagonistic distribution of H3K27me3 and H3K36me3, we wonder how H3K36me3 is distributed in H3K27me3 islands. We selected one area in each H3K27me3 island to visualize the distribution of H3K27me3 and H3K36me3. The diagram showed that H3K27me3 and H3K36me3 seldom co-existed at the same gene (Fig. 2h, Fig. S4h), suggesting that they may exclude each other. Indeed, the long H3K27me3 regions are

disrupted due to the deposition of H3K36me3. Thus, we speculate that there should be much more and longer H3K27me3 regions than expected in sorghum. As H2A.Z deposition can also extend to generate long H2A.Z regions (data not shown) and H2A.Z is absent in the gene body regions marked by H3K36me3 (Fig. 2e), we randomly selected three long H2A.Z regions and we found that enrichment of H3K36me3 excluded H2A.Z in these regions (Fig. 2i, Fig. S4i). However, the antagonistic relationship between H3K36me3 and H2A.Z is not as rigorous as H3K36me3 and H3K27me3, as at some loci H3K36me3 and H2A.Z co-existed. Taken together, these data suggest that H3K36me3 inhibits the deposition of both H3K27me3 and H2A.Z. To confirm whether the scenario is conserved in plants, we performed the similar analysis in *Arabidopsis* and rice. The results also revealed the antagonistic distributions between H3K27me3 and H3K36me3 as well as H2A.Z and H3K36me3 (Fig. S5a-d).

Dynamic change of histone marks during development in sorghum

In order to identify which histone marks are more likely to be related with specific gene expression during developmental processes, correlation analysis of differential enrichment of histone marks and gene expression in leaf and root was performed. The metaplots indicated that the overall levels of H3K9ac, H3K27ac, H3K4me3 and H3K36me3 were increased both at root-up-DEGs (Gene expression is up-regulated in roots compared to leaves) in root and leaf-up-DEGs (Gene expression is up-regulated in leaves compared to roots) in leaf (Fig. 3a). The number of genes whose expression changes were positively correlated with changes in these marks was much greater than the number of genes whose expression was negatively correlated with them (Fig. 3b). These supports the positive role of these marks in the regulation of gene expression. In contrast, H2A.Z, H3K4me2 and H3K37me3 levels were significantly decreased at root-up-DEGs in root but slightly decreased at leaf-up-DEGs in leaf (Fig. 3a), and genes negatively regulated by these marks were more than those positively regulated (Fig. 3b), suggesting negative correlation of these marks with gene expression.

To investigate how different histone marks cooperate to regulate root-leaf-DEGs (differentially expressed genes between root and leaf), we calculated the proportions of genes that were co-regulated by two histone marks. Considering the opposite roles of different histone marks in gene regulation as described above, the number of genes with increased H3K9ac, H3K27ac, H3K4me3, H3K36me3 or decreased H2A.Z, H3K4me2, H3K27me3

between leaf and root were used for the calculation. The higher proportions of overlapping (more than 30%) were observed between the increase of H3K9ac and the other active marks (H3K27ac, H3K4me3 and H3K36me3) as well as the increase of H3K4me3 and H3K36me3 in both leaf (vs root) and root (vs leaf) (Fig. 3c), suggesting that these histone marks tend to activate gene expression collaboratively. The decrease of H3K4me2 and H3K27me3 also showed a high percentage (30.63%) of overlapping only in leaf (vs root) (Fig. 3c), which demonstrates that they cooperate to repress more gene expression in root. We found that the proportions of overlapping between the increase of H3K36me3 and the decrease of H3K27me3 as well as the decrease of H2A.Z deposition were not as high as expected (8.57% and 15.69% in leaf (vs root), 8.15% and 10.15% root (vs leaf)) (Fig. 3c). This indicates that H3K36me3 enrichment contribute to small part of decline of H3K27me3 enrichment or H2A.Z deposition. In addition, the heat map showed that nearly half of genes with increased H3K36me3 were not marked with H3K27me3 (Fig. 3d). However, most of strong H3K27me3 enrichment were inhibited by the increase of H3K36me3. Similarly, the relatively higher levels of H2A.Z deposition were decreased to moderate levels after H3K36me3 enrichment was increased (Fig. 3e). These results further support the notion that H3K36me3 play part of the roles in the inhibition of H3K27me3 enrichment or H2A.Z deposition.

As shown in Fig. 3a, the differential enrichment of H3K27me3 in root-up-DEGs and leaf-up-DEGs in leaf and root was also obvious outside the gene body region (upstream of TSS and downstream of TES), suggesting that the dynamic change of H3K27me3 could spread outside the intragenic region. Alternatively, H3K27me3 deposition changes in units of long segments instead of single genes. To confirm the suspicion, we examined the number of H3K27m3 peaks with different length differentially enriched in root and leaf and found that although most of differentially enriched H3K27me3 peaks were short (less than 10 kb), more than 300 long H3K27me3 regions (more than 10 kb), consisting of 278 (10-20 kb), 87 (20-40 kb), 12 (40-60 kb), 5 (60-80 kb) and 4 (80-100 kb), were also differentially deposited (Fig. S6a). Genome-wide screenshots indicated that the changes of long H3K27me3 regions scattered in 10 chromosomes and negatively co-related with gene expression in general (Fig. S6b). But close observation on individual regions showed that a number of genes covered by long H3K27me3 regions were not activated despite removal of H3K27me3 (Fig. S6b). For

example, two neighboring long H3K27me3 regions decreased in root and localized in chr5:70,880 kb-71,000 kb cover 11 genes, among which only 3 genes were up-regulated (Fig. S6b). This suggests that the alteration of H3K27me3 enrichment in long regions is not always associated with transcriptional activity.

Leaf-specific expression of photosynthesis genes and root-specific expression lignin biosynthesis genes involves epigenetic regulation

The Kyoto Encyclopedia of Genes and Genomes (KEGG) and Gene Ontology (GO) analysis of root-leaf-DEGs with changed histone marks were performed to discover which pathways were more likely to be subjected to epigenetic regulation. The result showed that leaf-up-DEGs with various changed histone marks were enriched in photosynthesis pathway and localized to chloroplast or plastid. The root-up-DEGs were enriched in Phenylpropanoid biosynthesis pathway and localized to cell wall (Fig. 4a and Fig. S7). For a more detailed analysis of which genes in these pathways were epigenetically regulated, we investigated changes of expression and histone marks of all the photosynthesis genes encoding Photosystem I, Photosystem II, Cytochrome b6/f, ATP synthase, plastocyanin, cytc6 as well as chlorophyll biosynthesis genes. We found that expression of most photosynthesis genes and chlorophyll biosynthesis genes encoding the enzymes that catalyze the reactions from protoporphyrin IX to chlorophyll was dramatically increased in leaf (Fig. 4b). The increased expression of these genes was strongly associated with increased enrichment of H3K9ac, H3K27ac, H3K4me3 and H3K36me3, and partially with decreased enrichment H2A.Z, H3K4me2 and H3K27me3 (Fig. 4b). In particular, dynamic change of H3K27me3 occurred only on a very small proportion of these leaf-specific genes. Besides, a few of these genes were marked with high level of H3K27me3 in root (data not shown), suggesting that H3K27me3 is not required for repression of most of photosynthesis genes in root compared to the other histone marks.

As sorghum is a C4 plant, we would like to learn how C4 genes are regulated by different histone marks. In sorghum there were nine C4 genes: *carbonic anhydrase 2* (*CA2*), *CA3*, *NADP-malate dehydrogenase 2* (*NADP-MDH2*), *nicotinamide adenine dinucleotide phosphate (NADP)-malic enzyme 2* (*NADP-ME2*), *phosphoenolpyruvate carboxylase 6* (*PEPC6*), *PEPC kinase 2 (PPCK2*), *pyruvate orthophosphate dikinase 2* (*PPDK2*), *PPDK*

regulatory protein 1 (*PPDK-RP1*) and *RbcS* (Tao et al. 2020). We observed that seven C4 genes (except *CA3* and *PPCK2*) exhibited strong leaf expression specificity, and were mostly associated with differential enrichment of H3K9ac, H3K4me3 and H3K36me3 (Fig. 4c and 4d). Among these histone marks, H3K4me3 varied more significantly than the other marks, implying that H3K4me3 acts as the major epigenetic mark for the leaf-specific regulation of C4 gene expression. In addition, similar to the other photosynthesis genes, H3K27me3 was negatively associated with the expression of *CA2* and *PEPC6* only (Fig. 4c and 4d), suggesting a limited regulatory role of H3K27me3 on C4 genes. By contrast, the non-C4 genes homologous to C4 genes showed weaker leaf expression specificity and fewer of them were regulated by dynamic change of histone marks (Fig. 4c). These results suggest that the active histone marks may confer the leaf expression specificity of photosynthesis genes in sorghum.

When we looked into the root-up-DEGs with differentially enriched histone marks in the Phenylpropanoid biosynthesis pathway, we found many of these genes encode lignin biosynthesis enzymes, especially peroxidases (PODs) (data not shown). Therefore, we examined changes of expression and histone marks of all the lignin biosynthesis genes (Fig. 5a). It was shown that for 20 of 52 lignin biosynthesis genes, up-regulation of them in root involves dynamic change of at least one histone mark (Fig. 5b). And the epigenetically regulated genes encode all the enzymes for lignin biosynthesis except C3H, echoing the importance of epigenetic regulation in the lignin biosynthesis in root. More interestingly, we found that vast majority of *POD* genes showed root expression specificity that were associated with most of histone marks (Fig. 5c), although it is not clear how many of them are involved in lignin biosynthesis, especially in root. Particularly, all the 7 histone marks were differentially enriched on four *POD* genes (Fig. 5d). However, It seems that H3K36me3 is not involved in the regulation of most *POD* genes, as they were not marked with H3K36me3 even when they were significantly up-regulated in root (Fig. 5c). Unlike photosynthesis genes, we found decreased enrichment of H3K27me3 on considerable *POD* genes (Fig. 5c), suggesting that repression of these *POD* genes concerns H3K27me3.

Gene regulation in response to drought stress concerns histone marks except H3K36me3 and H3K27me3

To explore how histone marks engage in the induction of drought-responsive genes, we investigated the levels of histone marks in PEG-up-DEGs and PEG-down-DEGs in response to PEG treatment in root and leaf. The metaplots showed that PEG treatment only slightly affects the overall levels of some histone marks (Fig. 6a and 6b). For example, H3K9ac, H3K27ac, H3K4me3, H3K36me3 levels in PEG-up-DEGs in leaf and H3K36me3 level in PEG-up-DEGs in root showed a little increase. H3K9ac and H3K27ac levels in PEG-down-DEGs in leaf and root was slightly decreased. H2A.Z and H3K4me3 levels in PEG-down-DEGs in leaf and root rose and H2A.Z level in PEG-up-DEGs in leaf and root declined. These results are consistent with the regulatory roles of these marks. Then we performed association analysis of changes of histone marks and gene expression. In both leaf and root, only a few genes had altered H3K36me3 and H3K27me3 responding to PEG treatment (Fig. 6c and 6d), which suggests that these two marks are probably not involved in the PEG-responsive gene expression regulation. H3K4me3 was more likely to be associated with gene activation in response to PEG treatment, as the number of genes with increased H3K4me3 levels and gene expression in leaf (n = 138) and root (n = 363) was far more than the number of genes with the other relationships between H3K4me3 and gene expression (Fig. 6c and 6d). H3K9ac and H3K27ac were associated with either gene activation or repression when the level of these marks was increased or decreased responding to PEG treatment in leaf and root (Fig. 6c and 6d). Surprisingly, for certain number of genes in root but few in leaf changes of H3K9ac and H3K27ac were negatively correlated with changes of gene expression, which seems to contradict to the positive role of these marks. Finally, H2A.Z and H3K4me2 were negatively associated with some gene activation or repression in leaf and root (Fig. 6c and 6d). These results demonstrate that only a small proportion of gene induction in response to PEG treatment require dynamic change of histone marks.

In order to find out whether histone marks affect the degree of gene induction by PEG treatment, we classified PEG-up-DEGs into three groups: genes without enrichment of histone marks, genes with unchanged histone marks after PEG treatment, genes with changed histone marks after PEG treatment, and investigated fold change of each group gene expression. As PEG-responding gene up-regulation are more associated with increase of H3K9ac, H3K27ac, H3K4me3 and decrease of H2A.Z, the effect of these marks on gene

induction was analyzed. We found that the degree of induction of the genes with changed histone marks after PEG treatment was significantly higher than that of the other groups (Fig. S8), suggesting that the dynamic change of histone marks can elevate gene induction to some extent. However, the genes with unchanged H3K9ac, H3K27ac and H3K4me3 were induced to a relatively lower level than the genes without histone marks (Fig. S8). Conversely, the genes with unchanged H2A.Z enrichment were induced to a higher level (Fig. S8). These results demonstrate that the basic level of histone marks is not related to the gene responsiveness.

The direct regulation of many stress genes by transcription factors has been characterized in different plant species such as the genes involved in abscisic acid (ABA) metabolism, signaling and reactive oxygen species (ROS)-related and aquaporins, *late embryogenesis abundant* (LEA), wax biosynthese, polyamine biosynthesis genes (Hu et al. 2022). We found that induction of some of these stress genes also involves epigenetic regulation. For example, *9-cis-epoxycarotenoid dioxygenase 3* (*NCED3)*, the key gene in ABA biosynthesis pathway, and *delta1-PYRROLINE-5-CARBOXYLATE SYNTHASE 1* (*P5CS1)*, the key gene in proline biosynthesis pathway, were up-regulated by PEG treatment in both leaf and root (Table S2). The up-regulation was associated with the increase of H3K9ac, H3K27ac and H3K4me3 (Table S2). Surprisingly, expression of 9 in 10 clade A type 2C protein phosphatases (*PP2Cs*) genes, the repressors of ABA signaling, was also increased (Table S2), which usually entails increased enrichment of H3K9ac, H3K27me3, H3K4me3 and decreased enrichment H2A.Z in leaf and root. In addition, epigenetic regulation of many *LEA* genes in response to PEG was also observed (Table S2), although the scenario was different between leaf and root. The expression of these *LEA* genes was induced to a higher degree in leaf where change of epigenetic marks was more significant (Table S2). It is of great interest to ascertain if the higher degree of *LEA* expression is determined by changed epigenetic marks, and whether the differential induction of *LEA* genes in leaf and root has some physiological significance.

Dynamic change of histone marks is not necessary for the response of tissue-specific genes to drought stress

To learn that for the genes both differentially expressed between leaf and root and

responsive to PEG treatment whether the histone marks also change in both conditions (developmentally regulated and PEG responsive), we identified 780 and 2825 Root-up-DEGs that were also PEG-up-DEGs in leaf and PEG-down-DEGs in root respectively, 1359 and 950 Leaf-up-DEGs that were also PEG-down-DEGs in leaf and PEG-up-DEGs in root respectively (Fig. 7a), which were defined as four groups of common DEGs. Then we investigated the number of genes where histone marks changed uniquely in each condition or in both conditions among each of four groups of common DEGs. For the up-regulated genes increase of H3K9ac, H3K27me3, H3K4me3, H3K36me3 and decrease of H2A.Z, H3K4me2, H3K27me3 were analyzed, and for the down-regulated genes decrease of H3K9ac, H3K27me3, H3K4me3, H3K36me3 and increase of H2A.Z, H3K4me2, H3K27me3 were analyzed. The results revealed that for all four groups of common DEGs, the number of genes with change of histone marks uniquely regulated developmentally was much greater than those uniquely responsive to PEG and those in both conditions (Fig. 7b). Moreover, we found some common DEGs where 7 histone marks changed developmentally but none of them changed in response to PEG (Fig. S9). In particular, as we revealed that leaf-specific expression of photosynthesis genes and root-specific expression of lignin biosynthesis genes were associated with dynamic change of histone marks, we attempt to understand how these gene expression was affected by stress. We found that many photosynthesis genes including four C4 genes and lignin biosynthesis genes were slightly down-regulated (Fig. 7c and 7d, Fig. S10), and more than half of *POD* gene expression was decreased to a varying degree after PEG treatment (Fig. 7e). However, histone marks on only a small proportion of these genes were decreased. This indicates that dynamic change of histone marks important for tissue-specific regulation of gene expression is not necessary for the gene induction in response to environmental cues, and some tissue-specific regulatory factors are possibly required for the alteration of histone marks.

Cis-elements enriched in the promoter of genes with changed histone marks

Through above observations that the responses of chromatin dynamics to developmental or environmental cues were distinct in leaf and root, we considered that tissue-specific factors may direct the change of chromatin structure. Transcription factors (TFs) are the best candidates for the directing factors. *Cis*-elements analysis of promoter of genes (1.5kb

upstream from TSS) with changed histone marks was performed to predict which kinds of TFs are responsible for directing the writing or erasing of histone marks in different tissues. The five most enriched *cis*-elements for each variation of histone marks were shown in Fig. 8. For developmental genes, the *cis*-elements of Dof, AT-hook, MADS families TFs were associated with most of histone mark variations (Fig. 8a), suggesting that they were generally involved in the deposition or removal of histone marks in different tissues. The C2H2 Zinc finger TFs binding *cis*-element was inclined to be enriched in the genes with down-regulated histone marks in leaf (Fig. 8a), making it a good candidate as the tissue-specific guider for changing histone marks. In addition, ARID/BRIGHT TFs were responsible for some of histone mark variation (Fig. 8a). More specifically, YABBY TFs were associated with deposition of H3K36me3 in leaf (Fig. 8a). For PEG-induced genes, Dof, AT-hook, C2H2 Zinc finger and AP2 TFs were identified to be the most enriched *cis*-elements binding TFs (Fig. 8b). The bZIP TFs were more likely to be associated with up-regulation of H3K4me3 in leaf (Fig. 8b). MADS box *cis*-element was mostly enriched in the genes with decreased H3K9ac in leaf (Fig. 8b).

Discussion

The unique feature of H3K27me3 enrichment and function in sorghum

In this study we investigate the genome-wide enrichment of histone marks including H3K9ac, H3K27ac, H3K4me3, H3K36me3, H3K4me2, H3K27me3 and H2A.Z in sorghum. As reported in other plants, the distribution patterns of these marks in intragenic region are conserved in sorghum. For instance, H3K9ac, H3K27ac and H3K4me3 tend to be enriched in the TSS region, and H3K36me3, H3K4me2, H3K27me3 and H2A.Z were distributed in the whole transcribed region (Fig. 1a and 1b). However, early report revealed that H3K27me3 enrichment peaks in *Arabidopsis* was much shorter than that in animals (usually 20-50kb) and limited to single genes mostly (Zhang et al. 2007). But our analysis in *Arabidopsis*, rice and sorghum indicates that there are considerable long H3K27me3 regions in these species despite much less than the short regions (Fig. 2a and Fig. S3a). The maximum length of H3K37me3 region can reach more than 200 kb in sorghum. These results suggest that H3K27me3 enrichment can also spread to a long region covering multiple genes in plants. In Drosophila,

spreading of H3K27me3 requires specific *cis*-regulatory sequences, called Polycomb response elements (PREs) and pre-existing H3K27me3 (Margueron et al. 2009). In mammalian, spatially interacted nucleation sites are targeted by PRC2 complex to create H3K27me3-forming Polycomb foci for initiation of H3K27me3 spreading (Oksuz et al. 2018). Indeed, we found four H3K27me3 islands where the long H3K27me3 regions were clustered on three chromosomes of sorghum but not in *Arabidopsis* and rice (Fig. 2c and Fig. S3c). It is intriguing to unveil whether the H3K27me3 islands in sorghum are generated by spreading from PREs as in Drosophila or nucleation sites as in mammalian in the future. It has been disclosed that H3K27me3-mediated chromatin interaction takes place in *Arabidopsis* (Huang et al. 2021; Yang et al. 2022), but whether the interaction of chromatin is the prerequisite for H3K27me3 spreading remains to be elucidated. In our opinion, analysis of 3D genome structure of sorghum to reveal whether the four H3K27me3 islands are interacted is necessary for the next step. Besides, LIKE HETEROCHROMATIN PROTEIN 1 (LHP1), the reader of H3K27me3 in plant, has been reported to be responsible for the spreading of H3K27me3 towards the 3' end of the gene body in *Arabidopsis* (Veluchamy et al. 2016). It is of great importance to investigate whether the homolog of LHP1 in sorghum is involved in the spreading of H3K27me3 enrichment to a longer region.

H3K36me3 deposition inhibit both H3K27me3 and H2A.Z enrichment

Inhibition of PRC2 activity by H3K36m3 has been reported in animal and plant by biochemical analysis (Yuan et al. 2011; Yang et al. 2014), but whether H3K36me3 can serve as an active mark to restrict H3K27me3 spreading is not clear. Comparative analysis of genome-wide distribution of the two marks is missing. Here, by comparing genome-wide distribution of 7 histone marks in intragenic regions we found that gene-body-enriched H3K27me3 is depleted in the genes marked with H3K9ac, H3K27ac, H3K36me3 (Fig. 3a, 3b and 3d). But among these active marks only H3K36me3 is distributed in the entire gene body region which is similar to the distribution pattern of H3K27me3 (Fig. 3d and 3g), making it a suitable marker for inhibiting H3K27me3 deposition. When we visualized H3K36me3 enrichment in H3K27me3 island, we obtained mutually exclusive distribution patterns of H3K27me3 and H3K36me3 (Fig. 3h). In the long H3K27me3 regions, a gap would be present where H3K36me3 is deposited, indicating the inhibitory effect of H3K36me3 deposition on

H3K37me3 modification. But on the other hand, this also demonstrates that H3K36me3 cannot prevent the spreading of H3K27me3 since H3K27me3 is abundant at both sides of H3K36me3 region. It is of great interest to explore how H3K27me3 spreads over H3K36me3 regions. We also observed that strong enrichments of H3K36me3 were most associated with weak H2A.Z enrichments in the TSS region but hardly associated with gene-body-enriched H2A.Z (Fig. 3d and 3e). This reminds us of the antagonistic relationship between H2A.Z and DNA methylation in *Arabidopsis* (Zilberman et al. 2008). We found that similar to H3K27me3, strong enrichment of H3K36me3 disrupted the long H2A.Z regions (Fig. 3i), documenting that the enrichment of H3K36me3 also inhibit H2A.Z deposition. In mammals, H3K36me2/3 serves as platform to recruit DNMT3A for DNA methylation in the gene body in order for preventing spurious transcription initiation (Yano et al. 2022), but the scenario has not been revealed in plants. It is possible that one of the main functions of H3K36me3 and DNA methylation is to promote gene body H2A.Z eviction in plants. In *Arabidopsis* enrichment of H3K27me3 and deposition of H2A.Z are mutually reinforced (Carter et al. 2018), raising the possibility that the active marks H3K36me3 and DNA methylation can counteract both H2A.Z and H3K27me3. However, our results showed that H3K36me3 variation overlapped with part of changes of H2A.Z and H3K27me3 between leaf and root (Fig. 4c), suggesting that H3K36me3 deposition is not the main cause of removal of H2A.Z and H3K27me3.

The role of histone marks in the regulation of tissue-specific and stress-responsive genes in sorghum

We compared genome-wide enrichment of histone marks in leaf and root to unravel to what extent do histone marks affect transcriptional reprogramming of tissue-specific genes. The number of differential intragenic enrichments of each histone marks is much less than that of DEGs, suggesting that specific genes were epigenetically regulated in response to developmental cues. A large number of photosynthesis genes including C4 genes and lignin biosynthesis genes were among these genes (Fig. 4b-4d, Fig. 5b). The photosynthesis genes exhibit leaf-specific expression which is consistent with their function. Epigenetic regulation of some C4 genes have been reported in several species including sorghum (Offermann et al. 2006; Heimann et al. 2013; Li et al. 2017). Here we reported differential enrichment of

histone marks, particularly H3K4me3, on all C4 genes except PPCK2 in leaf and root of sorghum. But the homologous non-C4 genes were not expressed in a leaf-specific pattern and fewer of them were associated with change in histone marks. This suggest that the introduction of epigenetic marks onto C4 genes during evolution of C4 plants may be critical for their leaf-specific expression pattern. The single cell ChIP analysis is further required to determine whether cell-type-specific expression of C4 genes is conferred by cell-type-specific H3K4me3 enrichment, as C4 genes show mesophyll or bundle sheath cell-type-specificity in leaf. Many lignin biosynthesis genes showed root-specific expression. In sorghum, it has been reported that mutation of *brown midrib 12* (*bmr12*), which encodes caffeic acid O-methyltransferase (COMT) and is one of the key enzymes in lignin biosynthesis, leads to reduced lateral root density and altered root anatomy (Saluja et al. 2021). In this study, we revealed that activation of *bmr12* (SORBI_3007G047300) in root mainly implicated the increase of H3K4me3, H3K36me3 and the decrease of H3K27me3. We also identified many *POD* genes that showed strong root-specific expression pattern and were regulated by various histone marks, although whether they are involved in lignin biosynthesis remains to be elucidated. These results indicate that lignin biosynthesis under epigenetic regulation is important for sorghum root development. However, considering the multiple function of PODs (Cosio and Dunand 2009), it is very likely that they control root development through other pathways instead of lignin biosynthesis. Indeed, the role of POD in root development has been characterized in *Arabidopsis* (Marzol et al. 2022).

The dynamic change of histone marks in response to PEG in leaf and root was also compared in this study. H3K9ac, H3K27ac, H3K4me3, H3K4me2, and H2A.Z are associated with gene induction in varying degree in response to PEG (Fig. 5a-5d). The fold changes of the genes with changed histone marks were greater than those of the genes with unchanged histone marks or without enrichment of histone marks (Fig. S8), suggesting that the variation of histone marks can improve the degree of gene induction. However, H3K36me3 and H3K27me3 enrichments in few DEGs changed both in leaf and root after PEG treatment (Fig. 5c and 5d), suggesting that these two marks are probably not involved in PEG-responsive gene regulation in the process of response in sorghum. The study in moss Physcomitrella patens also showed that H3K27me3 change was not significant in response to drought stress

(Widiez et al. 2014). However, in *Arabidopsis* salt priming results in shortening and fractionation of H3K27me3 islands (Sani et al. 2013). The H3K27me3 dynamics responding to salt and cold stress has also been revealed in rice (Zheng et al. 2019; Dasgupta et al. 2022). These demonstrate that different stress signals in different species induce distinct responses of H3K27me3 landscape.

Materials and methods

Plant growth conditions and PEG treatment

Sorghum (BTx623 variety) seeds were surface-sterilized and then soaked for germination. The germinated seeds were transferred to the nursery box (1/2 MS) to continue growing in a growth room kept at 28□ with a 12h light/12 dark cycle. The 14-day-old seedlings were transferred to the nursery box containing 20% PEG6000 that was prepared with 1/2 MS. The seedlings transferred to fresh 1/2MS solution was used as the control. After 6 hours treatment, the third leaves and roots were harvested respectively for subsequent experiments.

RNA-seq

The leaves and roots were harvested and frozen immediately in liquid nitrogen. Total RNA was extracted using TRNzol Universal Reagent (TIANGEN) following the manufacturer's instructions. The quality of RNA was measured by gel electrophoresis, Nanodrop analyzer, Labchip and Qubit analyzer respectively. mRNA was purified by using oligo(dT) and then fragmented by incubating in fragmentation buffer. The fragmented mRNA was primed with random hexamer primers and reverse-transcribed with Reverse Transcriptase. After end repair, adenylation, adaptor ligation, purification,PCR amplification, and quality control, sequencing was performed on an Illumina HiSeq system.

ChIP-seq

Chromatin immunoprecipitation (ChIP) was performed as described in Hu et al. (Hu et al. 2020), In brief, the samples were crosslinked with 1% (v/v) formaldehyde. The nuclei were extracted and the chromatin DNA was broken into 200-500bp fragments by sonication (Soniprep 150, energy 5, 15s on and 1min off for 5 times). The antibodies H3K9ac (07-352, Millipore), H3K27ac (07-360, Millipore), H3K4me2 (07-030, Millipore), H3K4me3 (07-473,

Millipore), H3K27me3 (A2363, ABclonal), H3K36me3 (ab9050, abcam), H2A.Z (preparation using antigen "GKGLLAAKTTAAKSAEKDKGKKAPV") were incubated with Protein A agarose (16-157, Millipore) before mixed with sonicated chromatin. The immunoprecipitated DNA was purified for constructing libraries and sequenced on an Illumina HiSeq system.

Raw sequencing reads filtering.

To obtain high quality clean reads of RNA-seq, ChIP-seq and MNase-seq, the raw sequencing reads were trimmed by Trimmomatic v0.32 (https://github.com/usadellab/Trimmomatic) with parameters of "TruSeq3-PE.fa:2:30:10 LEADING:20 TRAILING:20 SLIDINGWINDOW:4:15 MINLEN:36".

Analyses of RNA-seq data.

Transcript abundance was quantified using pseudoalignment of high quality clean RNA-seq reads to the reference cDNA sequences and gene models from Sorghum_bicolor_NCBIv3 assembly of the variety BTx623 (McCormick et al. 2018), as implemented in Kallisto (v0.48.0) (Bray et al. 2016). The output pseudoalignment bam files were converted to bigwig format using "bamCoverage" tool of deepTools (v3.5.0) (Ramirez et al. 2016). Differentially expressed genes (DEGs) were identified using DESeq2 v1.22 (Love et al. 2014), genes with TPM value higher than 1 in all the three replicates of each sample were regarded as expressed genes, genes with |log2 (Fold change)| > 1, *P* adjust value < 0.05 and at least expressed in one sample were regarded as DEGs.

Analyses of ChIP-seq data.

High quality clean reads were aligned against the reference Sorghum_bicolor_NCBIv3 genome assembly using Bowtie2 (v2.4.4) (Langmead and Salzberg 2012). Aligned reads with MAPQ < 5 were filtered using SAMtools (v1.9) (Li et al. 2009). Duplicated alignments were removed using Picard (v2.23.9) (http://broadinstitute.github.io/picard/). Before peak calling, the extsize were predicted by phantompeakqualtools (v1.2.2) (Landt et al. 2012). Narrow peaks of H3K9ac, H3K27ac and H3K4me3 ChIP-seq reads densities were identified using MACS2 (v2.2.7.1) (Zhang et al. 2008) with parameters "-f BAM -p 1e-5 --mfold 2 20 --nomodel --extsize $spp_result --to-large". The input control were used by added parameter "-c". For broad peaks calling including H3K4me2, H3K27me3, H3K36me3 and KH2A.Z, the "--broad" parameter was added. The peaks from biological replicate samples were merged by BEDTools (v2.27) (Quinlan and Hall 2010), two replicate bam files were merged by SAMTools. We then extracted the reads from the merged bam files that mapped on the merged peaks using BEDtools, and converted the output new bam files to RPKM normalized bigwig files by deepTools. The metaplot and heat map profiles of epigenetic and genomic features were generated and plotted by deepTools.

The signal portion of tags (SPOT) and the fraction of reads in called peak regions (FRiP) value were calculated using Hotspot v4.1.0 (https://github.com/rthurman/hotspot) and commands in-house. To assess the repeatability between biological samples, we calculated the correlation coefficients between samples using deepTools. The visualization of reads coverage is available on http://crispr.hzau.edu.cn/cgi-bin/CRISPR-Cereal/gb2/gbrowse/Sorghum_bicolor/.

Visualization of overall signals.

All types of signals were visualized using Circos (version 0.69) (Krzywinski et al. 2009) with the commands available on github (https://github.com/hcph/Sorghum-omics-dataset-analysis).

Analyses of H3K27me3 regions.

The H3K27me3 peaks in bed files and the signal normalized bigwig files were downloaded from the ChIP-hub databases (Fu et al. 2022) using the sample ID of SRX7734769 and SRX7734770 for *Arabidopsis*, and SRX7426661 and SRX7426662 for rice. Peaks in the two replicates with 1 bp overlap (MG0) as well as overlap regions lower than 1,000 bp (MG1000) were merged using BEDTools. The number of H3K27me3 regions with different length distributedwere visualized. To investigate the distribution of H3K27m3 regions with different number of overlapped genes, we firstly found the overlapped genes for each H3K27me3 region, then the number of overlapped genes was calculated. The *Arabidopsis* and rice H3K27me3 regions longer than 10 kb were extracted and the H3K27me3 signal located in these regions were visualized using pyGenomeTracks v3.5 (Lopez-Delisle et al. 2021).

Detection of differentially histone modified genes (DMGs).

Reads mapped to genes were extracted as described before. The reads density on each genes was calculated by Subread v2.0.0 (Liao et al. 2013). The TPM value was used to quantified the reads density on each gene, followed by DMGs detection using DeSeq2. Genes with TPM value higher than 10 in the two replicates were regarded as modified genes, and genes with |log2 (Fold change)| > 0.75, *P* adjust value < 0.05 and at least being modified in one sample were regarded as DMGs. The pearson correlation coefficients for the differentially modification and expression levels was calculated. Long (>10 kb) H3K27me3 signals located in differentially H3K27me3 modified regions were extracted with BEDtools as described before, the extracted H3K27me3 signal and the corresponding gene expression signal were visualized with Circlize v0.4.15 (Gu et al. 2014) .

Analyses of relationship between different histone modifications.

The signal matrix of the seven histone modification marks was built by deepTools using the merged and RPKM normalized bigwig files as input. The signal of a single mark was used in turn as a template for clustering the signals of the remaining marks into three groups. The datasets in rice (Zheng et al. 2019; Lu et al. 2020; Zhao et al. 2020) and *Arabidopsis* (Carter et al. 2018; Xi et al. 2020) were downloaded from ChIP-hub and analyzed in the same way as

in sorghum. The signals located in long peaks (> 10 kb) were extracted and visualized as described before.The number of DMGs with two differential types of histone modifications or only differentially in one histone modifications were calculated and visualized.

GO and KEGG enrichment analysis.

GO and KEGG enrichment was performed using g:Profiler (https://biit.cs.ut.ee/gprofiler/gost), the enriched GO terms and KEGG pathways were visualized using R package ggplot2 v3.3.5.

Motif enrichment.

The promoter sequences (upstream 1,500 bp) of DMGs were extracted using BEDTools. The sequences were submitted into the CentriMO (https://meme-suite.org/meme/tools/centrimo) online analysis toolkit for motif enrichment analysis. The "anywhere" mode was selected to perform local motif enrichment and the motif database was supported by CIS-BP v2.0 (Weirauch et al. 2014).

Declarations

Ethics approval and consent to participate

Not applicable

Consent for publication

Not applicable

Availability of data and materials

The ChIP-seq, MNase-seq and RNA-seq data generated in this article were deposited in the NCBI Sequence Read Archive (SRA) (http://trace.ncbi.nlm.nih.gov/Traces/sra/) under the BioProject accession number PRJNA952350.

Competing interests

The authors declare that they have no competing interests

Funding

This work was supported by Research Initiation Fund for High-level Talents of China Three Gorges University.

Authors' contributions

The project was conceived by YH and supervised by XS. YH performed ChIP-seq, MNase-seq and RNA-seq with help from QH, GZ, XQ and ZD. CH performed the bioinformatics analyses with help from YS and SB. The manuscript was drafted by YH and XS and revised by all the authors. ZH participate in the critical discussion. The authors read and approved the final manuscript.

Acknowledgements

We sincerely thank the computing platform of the National Key Laboratory of Crop Genetic Improvement in HZAU for providing the computational resources.

References

Barski A, Cuddapah S, Cui K, Roh TY, Schones DE, Wang Z, Wei G, Chepelev I, Zhao K. 2007. High-resolution profiling of histone methylations in the human genome. Cell 129 (4):823-837.

Blackledge NP, Klose RJ. 2021. The molecular principles of gene regulation by Polycomb repressive complexes. Nat Rev Mol Cell Biol 22 (12):815-833.

Bray NL, Pimentel H, Melsted P, Pachter L. 2016. Near-optimal probabilistic RNA-seq quantification. Nat Biotechnol 34 (5):525-527.

Carter B, Bishop B, Ho KK, Huang R, Jia W, Zhang H, Pascuzzi PE, Deal RB, Ogas J. 2018. The Chromatin Remodelers PKL and PIE1 Act in an Epigenetic Pathway That Determines H3K27me3 Homeostasis in Arabidopsis. Plant Cell 30 (6):1337-1352.

Cosio C, Dunand C. 2009. Specific functions of individual class III peroxidase genes. J Exp Bot 60 (2):391-408.

Dasgupta P, Prasad P, Bag SK, Chaudhuri S. 2022. Dynamicity of histone H3K27ac and H3K27me3 modifications regulate the cold-responsive gene expression in Oryza sativa L. ssp. indica. Genomics 114 (4):110433.

Ding Y, Ndamukong I, Xu Z, Lapko H, Fromm M, Avramova Z. 2012. ATX1-generated H3K4me3 is required for efficient elongation of transcription, not initiation, at ATX1-regulated genes. PLoS Genet 8 (12):e1003111.

Ernst J, Kheradpour P, Mikkelsen TS, Shoresh N, Ward LD, Epstein CB, Zhang X, Wang L, Issner R, Coyne M et al. 2011. Mapping and analysis of chromatin state dynamics in nine human cell types. Nature 473 (7345):43-49.

Finogenova K, Bonnet J, Poepsel S, Schafer IB, Finkl K, Schmid K, Litz C, Strauss M, Benda C, Muller J. 2020. Structural basis for PRC2 decoding of active histone methylation marks H3K36me2/3. Elife 9:e61964.

Fu LY, Zhu T, Zhou X, Yu R, He Z, Zhang P, Wu Z, Chen M, Kaufmann K, Chen D. 2022. ChIP-Hub provides an integrative platform for exploring plant regulome. Nat Commun 13 (1):3413.

Gates LA, Shi J, Rohira AD, Feng Q, Zhu B, Bedford MT, Sagum CA, Jung SY, Qin J, Tsai MJ et al. 2017. Acetylation on histone H3 lysine 9 mediates a switch from transcription

initiation to elongation. J Biol Chem 292 (35):14456-14472.

Gu Z, Gu L, Eils R, Schlesner M, Brors B. 2014. circlize Implements and enhances circular visualization in R. Bioinformatics 30 (19):2811-2812.

Guenther MG, Levine SS, Boyer LA, Jaenisch R, Young RA. 2007. A chromatin landmark and transcription initiation at most promoters in human cells. Cell 130 (1):77-88.

Heimann L, Horst I, Perduns R, Dreesen B, Offermann S, Peterhansel C. 2013. A Common histone modification code on C4 genes in maize and its conservation in Sorghum and Setaria italica. Plant Physiol 162 (1):456-469.

Hsu PL, Shi H, Leonen C, Kang J, Chatterjee C, Zheng N. 2019. Structural Basis of H2B Ubiquitination-Dependent H3K4 Methylation by COMPASS. Mol Cell 76 (5):712-723 e714.

Hu Y, Chen X, Shen X. 2022. Regulatory network established by transcription factors transmits drought stress signals in plant. Stress Biology 2 (1):1-22.

Hu Y, Lai Y, Chen X, Zhou DX, Zhao Y. 2020. Distribution pattern of histone marks potentially determines their roles in transcription and RNA processing in rice. J Plant Physiol 249:153167.

Huang Y, Sicar S, Ramirez-Prado JS, Manza-Mianza D, Antunez-Sanchez J, Brik-Chaouche R, Rodriguez-Granados NY, An J, Bergounioux C, Mahfouz MM et al. 2021. Polycomb-dependent differential chromatin compartmentalization determines gene coregulation in Arabidopsis. Genome Res 31 (7):1230-1244.

Iwamori N, Tominaga K, Sato T, Riehle K, Iwamori T, Ohkawa Y, Coarfa C, Ono E, Matzuk MM. 2016. MRG15 is required for pre-mRNA splicing and spermatogenesis. Proc Natl Acad Sci U S A 113 (37):E5408-5415.

Krzywinski M, Schein J, Birol I, Connors J, Gascoyne R, Horsman D, Jones SJ, Marra MA. 2009. Circos: an information aesthetic for comparative genomics. Genome Res 19 (9):1639-1645.

Landt SG, Marinov GK, Kundaje A, Kheradpour P, Pauli F, Batzoglou S, Bernstein BE, Bickel P, Brown JB, Cayting P et al. 2012. ChIP-seq guidelines and practices of the ENCODE and modENCODE consortia. Genome Res 22 (9):1813-1831.

Langmead B, Salzberg SL. 2012. Fast gapped-read alignment with Bowtie 2. Nat Methods 9 (4):357-359.

Lauberth SM, Nakayama T, Wu X, Ferris AL, Tang Z, Hughes SH, Roeder RG. 2013. H3K4me3 interactions with TAF3 regulate preinitiation complex assembly and selective gene activation. Cell 152 (5):1021-1036.

Li H, Handsaker B, Wysoker A, Fennell T, Ruan J, Homer N, Marth G, Abecasis G, Durbin R, Genome Project Data Processing S. 2009. The Sequence Alignment/Map format and SAMtools. Bioinformatics 25 (16):2078-2079.

Li Y, Dong XM, Jin F, Shen Z, Chao Q, Wang BC. 2017. Histone Acetylation Modifications Affect Tissue-Dependent Expression of Poplar Homologs of C(4) Photosynthetic Enzyme Genes. Front Plant Sci 8:950.

Li Y, Mukherjee I, Thum KE, Tanurdzic M, Katari MS, Obertello M, Edwards MB, McCombie WR, Martienssen RA, Coruzzi GM. 2015. The histone methyltransferase SDG8 mediates the epigenetic modification of light and carbon responsive genes in plants. Genome Biol 16 (1):79.

Liao Y, Smyth GK, Shi W. 2013. The Subread aligner: fast, accurate and scalable read mapping by seed-and-vote. Nucleic Acids Res 41 (10):e108.

Liu B, Wei G, Shi J, Jin J, Shen T, Ni T, Shen WH, Yu Y, Dong A. 2016. SET DOMAIN GROUP 708, a histone H3 lysine 36-specific methyltransferase, controls flowering time in rice (Oryza sativa). New Phytol 210 (2):577-588.

Lopez-Delisle L, Rabbani L, Wolff J, Bhardwaj V, Backofen R, Gruning B, Ramirez F, Manke T. 2021. pyGenomeTracks: reproducible plots for multivariate genomic datasets. Bioinformatics 37 (3):422-423.

Love MI, Huber W, Anders S. 2014. Moderated estimation of fold change and dispersion for RNA-seq data with DESeq2. Genome Biol 15 (12):550.

Lu Y, Tan F, Zhao Y, Zhou S, Chen X, Hu Y, Zhou DX. 2020. A Chromodomain-Helicase-DNA-Binding Factor Functions in Chromatin Modification and Gene Regulation. Plant Physiol 183 (3):1035-1046.

Margueron R, Justin N, Ohno K, Sharpe ML, Son J, Drury WJ, 3rd, Voigt P, Martin SR, Taylor WR, De Marco V et al. 2009. Role of the polycomb protein EED in the propagation of repressive histone marks. Nature 461 (7265):762-767.

Marzol E, Borassi C, Carignani Sardoy M, Ranocha P, Aptekmann AA, Bringas M,

Pennington J, Paez-Valencia J, Martinez Pacheco J, Rodriguez-Garcia DR et al. 2022. Class III Peroxidases PRX01, PRX44, and PRX73 Control Root Hair Growth in Arabidopsis thaliana. Int J Mol Sci 23 (10):5375.

McCormick RF, Truong SK, Sreedasyam A, Jenkins J, Shu S, Sims D, Kennedy M, Amirebrahimi M, Weers BD, McKinley B et al. 2018. The Sorghum bicolor reference genome: improved assembly, gene annotations, a transcriptome atlas, and signatures of genome organization. Plant J 93 (2):338-354.

Offermann S, Danker T, Dreymuller D, Kalamajka R, Topsch S, Weyand K, Peterhansel C. 2006. Illumination is necessary and sufficient to induce histone acetylation independent of transcriptional activity at the C4-specific phosphoenolpyruvate carboxylase promoter in maize. Plant Physiol 141 (3):1078-1088.

Oksuz O, Narendra V, Lee CH, Descostes N, LeRoy G, Raviram R, Blumenberg L, Karch K, Rocha PP, Garcia BA et al. 2018. Capturing the Onset of PRC2-Mediated Repressive Domain Formation. Mol Cell 70 (6):1149-1162 e1145.

Quinlan AR, Hall IM. 2010. BEDTools: a flexible suite of utilities for comparing genomic features. Bioinformatics 26 (6):841-842.

Ramirez F, Ryan DP, Gruning B, Bhardwaj V, Kilpert F, Richter AS, Heyne S, Dundar F, Manke T. 2016. deepTools2: a next generation web server for deep-sequencing data analysis. Nucleic Acids Res 44 (W1):W160-165.

Ringel AE, Cieniewicz AM, Taverna SD, Wolberger C. 2015. Nucleosome competition reveals processive acetylation by the SAGA HAT module. Proc Natl Acad Sci U S A 112 (40):E5461-5470.

Roudier F, Teixeira FK, Colot V. 2009. Chromatin indexing in Arabidopsis: an epigenomic tale of tails and more. Trends Genet 25 (11):511-517.

Saluja M, Zhu F, Yu H, Walia H, Sattler SE. 2021. Loss of COMT activity reduces lateral root formation and alters the response to water limitation in sorghum brown midrib (bmr) 12 mutant. New Phytol 229 (5):2780-2794.

Sani E, Herzyk P, Perrella G, Colot V, Amtmann A. 2013. Hyperosmotic priming of Arabidopsis seedlings establishes a long-term somatic memory accompanied by specific changes of the epigenome. Genome Biol 14 (6):R59.

Schmitges FW, Prusty AB, Faty M, Stutzer A, Lingaraju GM, Aiwazian J, Sack R, Hess D, Li L, Zhou S et al. 2011. Histone methylation by PRC2 is inhibited by active chromatin marks. Mol Cell 42 (3):330-341.

Schwartz YB, Kahn TG, Nix DA, Li XY, Bourgon R, Biggin M, Pirrotta V. 2006. Genome-wide analysis of Polycomb targets in Drosophila melanogaster. Nat Genet 38 (6):700-705.

Sequeira-Mendes J, Araguez I, Peiro R, Mendez-Giraldez R, Zhang X, Jacobsen SE, Bastolla U, Gutierrez C. 2014. The Functional Topography of the Arabidopsis Genome Is Organized in a Reduced Number of Linear Motifs of Chromatin States. Plant Cell 26 (6):2351-2366.

Sorenson MR, Jha DK, Ucles SA, Flood DM, Strahl BD, Stevens SW, Kress TL. 2016. Histone H3K36 methylation regulates pre-mRNA splicing in Saccharomyces cerevisiae. RNA Biol 13 (4):412-426.

Suzuki S, Kato H, Suzuki Y, Chikashige Y, Hiraoka Y, Kimura H, Nagao K, Obuse C, Takahata S, Murakami Y. 2016. Histone H3K36 trimethylation is essential for multiple silencing mechanisms in fission yeast. Nucleic Acids Res 44 (9):4147-4162.

Tao Y, George-Jaeggli B, Bouteille-Pallas M, Tai S, Cruickshank A, Jordan D, Mace E. 2020. Genetic Diversity of C(4) Photosynthesis Pathway Genes in Sorghum bicolor (L.). Genes (Basel) 11 (7):806.

Taverna SD, Ilin S, Rogers RS, Tanny JC, Lavender H, Li H, Baker L, Boyle J, Blair LP, Chait BT et al. 2006. Yng1 PHD finger binding to H3 trimethylated at K4 promotes NuA3 HAT activity at K14 of H3 and transcription at a subset of targeted ORFs. Mol Cell 24 (5):785-796.

Veluchamy A, Jegu T, Ariel F, Latrasse D, Mariappan KG, Kim SK, Crespi M, Hirt H, Bergounioux C, Raynaud C et al. 2016. LHP1 Regulates H3K27me3 Spreading and Shapes the Three-Dimensional Conformation of the Arabidopsis Genome. PLoS One 11 (7):e0158936.

Wang H, Fan Z, Shliaha PV, Miele M, Hendrickson RC, Jiang X, Helin K. 2023. H3K4me3 regulates RNA polymerase II promoter-proximal pause-release. Nature 615 (7951):339-348.

Weirauch MT, Yang A, Albu M, Cote AG, Montenegro-Montero A, Drewe P, Najafabadi HS, Lambert SA, Mann I, Cook K et al. 2014. Determination and inference of eukaryotic

transcription factor sequence specificity. Cell 158 (6):1431-1443.

Widiez T, Symeonidi A, Luo C, Lam E, Lawton M, Rensing SA. 2014. The chromatin landscape of the moss Physcomitrella patens and its dynamics during development and drought stress. Plant J 79 (1):67-81.

Xi Y, Park SR, Kim DH, Kim ED, Sung S. 2020. Transcriptome and epigenome analyses of vernalization in Arabidopsis thaliana. Plant J 103 (4):1490-1502.

Yang H, Howard M, Dean C. 2014. Antagonistic roles for H3K36me3 and H3K27me3 in the cold-induced epigenetic switch at Arabidopsis FLC. Curr Biol 24 (15):1793-1797.

Yang T, Wang D, Tian G, Sun L, Yang M, Yin X, Xiao J, Sheng Y, Zhu D, He H et al. 2022. Chromatin remodeling complexes regulate genome architecture in Arabidopsis. Plant Cell 34 (7):2638-2651.

Yano S, Ishiuchi T, Abe S, Namekawa SH, Huang G, Ogawa Y, Sasaki H. 2022. Histone H3K36me2 and H3K36me3 form a chromatin platform essential for DNMT3A-dependent DNA methylation in mouse oocytes. Nat Commun 13 (1):4440.

Yuan W, Xu M, Huang C, Liu N, Chen S, Zhu B. 2011. H3K36 methylation antagonizes PRC2-mediated H3K27 methylation. J Biol Chem 286 (10):7983-7989.

Zhang X, Clarenz O, Cokus S, Bernatavichute YV, Pellegrini M, Goodrich J, Jacobsen SE. 2007. Whole-genome analysis of histone H3 lysine 27 trimethylation in Arabidopsis. PLoS Biol 5 (5):e129.

Zhang Y, Liu T, Meyer CA, Eeckhoute J, Johnson DS, Bernstein BE, Nusbaum C, Myers RM, Brown M, Li W et al. 2008. Model-based analysis of ChIP-Seq (MACS). Genome Biol 9 (9):R137.

Zhao L, Xie L, Zhang Q, Ouyang W, Deng L, Guan P, Ma M, Li Y, Zhang Y, Xiao Q et al. 2020. Integrative analysis of reference epigenomes in 20 rice varieties. Nat Commun 11 (1):2658.

Zheng D, Wang L, Chen L, Pan X, Lin K, Fang Y, Wang XE, Zhang W. 2019. Salt-Responsive Genes are Differentially Regulated at the Chromatin Levels Between Seedlings and Roots in Rice. Plant Cell Physiol 60 (8):1790-1803.

Zilberman D, Coleman-Derr D, Ballinger T, Henikoff S. 2008. Histone H2A.Z and DNA methylation are mutually antagonistic chromatin marks. Nature 456 (7218):125-129.

805

Figure legends

Figure 1 Distribution pattern of histone marks in sorghum.

(a) Metaplots of 7 histone mark profiles of all genes in leaf and root before and after PEG treatment. **(b)** Heat maps of histone mark enrichment of intragenic region in leaf and root before and after PEG treatment. Black arrows indicate the TSS-enriched H3K27me3 present in leaf but not in root. Two-week-old sorghum seedlings were treated with 20% PEG6000 for 6 hours. Then root and leaf of control (without PEG treatment) and PEG-treated plants were harvested for ChIP-seq. **(c)** Length distribution of H3K27me3 regions in leaf and root. **(d)** The number of genes covered by each H3K27me3 region in leaf and root. "MG1000" indicates that the adjacent H3K27me3 regions were joined when they were separated by less than 1 kb while "MG0" indicates that they were not jointed. **(e)** Genome browser screen shots of 4 H3K27me3 islands on Chromosomes 2, 5, 8. H3K27me3 islands were defined as the areas where a number of long H3K27me3 regions clustered.

Figure 2 Analysis of overlapping enrichment of different histone marks in sorghum leaf.

The enrichment of H3K9ac **(a)**, H3K27ac **(b)**, H3K4me3 **(c)**, H3K36me3 **(d)**, H2A.Z **(e)**, H3K4me2 **(f)**, and H3K27me3 **(g)** in intragenic region were clustered into 3 categories (C1, C2 and C3) respectively and were put on the far left. The other 6 histone mark enrichment and gene expression level were shown next to the clustered marks. **(h)** Genome browser screen shots showing part of the areas in 4 H3K27me3 islands where H3K36me3 and H3K27me3 excluded from each other. **(i)** Genome browser screen shots showing some areas where H3K36me3 and H2A.Z excluded from each other.

Figure 3 Correlation analysis of differential enrichment of histone marks and differential gene expression in leaf and root.

(a) Metaplots of 7 histone mark profiles in differentially expressed genes (DEGs) between leaf and root. **(b)** Scatterplots of correlation between change of histone marks (log2FC-root vs leaf) and change of gene expression (log2FC-root vs leaf). Red dots represent the genes with both increased histone mark levels (log2FC > 0.75, $p < 0.05$) and increased expression levels (log2FC > 1, $p < 0.05$) and the genes with both decreased histone mark levels (log2FC < -0.75, $p < 0.05$) and decreased expression levels (log2FC < 1, $p < 0.05$) (Positive relationship). Blue dots represent the genes with increased histone mark levels and decreased expression levels

and the genes with decreased histone mark levels and increased expression levels (Negative relationship). Gray dots represent the genes in which correlation between change of histone marks and change of gene expression was not significant. The number of the co-related genes was indicated. **(c)** The proportion of genes in which two histone marks changes between leaf and root. “Former unique” means the genes in which the former one of the two compared histone mark shown on the horizontal axis change but the latter one does not. “Latter unique” means the genes in which the latter histone mark change but the former one does not. “Common” means the genes in which both histone marks change. **(d)** Heat maps of H3K27me3 and H3K36me3 enrichments in all the genes with changed H3K36me3 (left, H3K36me3 increases in root; right, H3K36me3 increases in leaf). **(e)** Heat maps of H2A.Z and H3K36me3 enrichments in all the genes with changed H3K36me3 (left, H3K36me3 increases in root; right, H3K36me3 increases in leaf).

Figure 4 Leaf-specific expression of photosynthesis genes is associated with dynamic change of histone marks.

(a) KEGG analysis of the leaf-up-DEGs and root-up-DEGs with differential enrichment of various histone marks in leaf and root. The pathways marked with pink background represent leaf-up-DEGs enriched Photosynthesis-related pathways. The pathway marked with purple background represents root-up-DEGs enriched Phenylpropanoid biosynthesis pathway. Heat maps showing fold change (log2FC) of expression and histone marks of photosynthesis genes **(b)** and C4 and non-C4 genes **(c)** in leaf compared to root. **(d)** Genome browser screen shots of histone mark enrichment on C4 genes in leaf and root.

Figure 5 Root-specific expression of lignin biosynthesis and POD genes is associated with dynamic change of histone marks.

(a) Schematic diagram of lignin synthesis. Heat maps showing fold change (log2FC) of expression and histone marks of photosynthesis genes **(b)** and C4 and non-C4 genes **(c)** in leaf compared to root. **(d)** Genome browser screen shots of histone mark enrichment on ten POD genes with topmost expression change in leaf and root.

Figure 6 Correlation analysis of changes of histone marks and gene expression in response to PEG treatment in leaf and root.

Metaplots of 7 histone mark profiles in differentially expressed genes (DEGs) in response to

PEG treatment in leaf **(a)** and root **(b)**. Scatterplots of correlation between change of histone marks (log2FC) and change of gene expression (log2FC) in response to PEG treatment in leaf **(c)** and root **(d)**. Red dots represent the genes with both increased histone mark levels (log2FC > 0.75, $p < 0.05$) and increased expression levels (log2FC > 1, $p < 0.05$) and the genes with both decreased histone mark levels (log2FC < -0.75, $p < 0.05$) and decreased expression levels (log2FC < 1, $p < 0.05$) (Positive relationship). Blue dots represent the genes with increased histone mark levels and decreased expression levels and the genes with decreased histone mark levels and increased expression levels (Negative relationship). Gray dots represent the genes in which correlation between change of histone marks and change of gene expression was not significant. The number of the co-related genes was indicated.

Figure 7 Dynamic change of histone marks in the genes that were both differentially expressed between leaf and root and in response to PEG treatment.

(a) Venn diagram of overlapping DEGs both between leaf and root and in response to PEG treatment. Four groups (I, II, III, IV) of the overlapping DEGs, also designated as the common DEGs, were identified. Root-up-DEGs: genes with increased expression in root compared to leaf; Leaf-up-DEGs: genes with increased expression in leaf compared to root; PEG-up-DEGs(leaf): genes with increased expression in response to PEG in leaf; PEG-down-DEGs(leaf): genes with decreased expression in response to PEG in leaf; PEG-up-DEGs(root): genes with increased expression in response to PEG in root; PEG-down-DEGs(root): genes with decreased expression in response to PEG in root. **(b)** The overlapping analysis of histone mark changes in four groups of the common DEGs identified in **(a)** both between leaf and root and in response to PEG treatment. “Unique” represents histone marks changed only in this condition but not the other while “common” means histone marks changed in both conditions. The number of “unique” or “common” genes was marked on the column. The total number of each group of the common DEGs was indicated. Heat maps showing fold change (log2FC) of expression and histone marks of photosynthesis genes **(c)** and C4 and non-C4 genes **(d)** before and after PEG treatment in leaf, and POD genes **(e)** before and after PEG treatment in root.

Figure 8 Cis-elements analysis of genes with histone marks changing between leaf and root (a) and in response to PEG treatment (b).

CL: Leaf control; PL: Leaf PEG treatment; CR: Root control; PR: Leaf PRG treatment. The percentage (%) of the genes possessing the cis-element relative to the total genes with the histone mark changing was marked on the column.

Figure S1. The quality of ChIP-seq and RNA-seq data obtained in this study.

Figure S2. The overview of genome-wide enrichment of histone marks in sorghum.

Figure S3. Long H3K27me3 regions in Arabidopsis and rice.

Figure S4. Analysis of overlapping enrichment of different histone marks in sorghum root.

Figure S5. The relationship between H3K36me3, H3K27me3 and H2A.Z in Arabidopsis and rice.

Figure S6. Long H3K27me3 peaks change between leaf and root

Figure S7 Gene Ontology (GO) analysis of the leaf-up-DEGs and root-up-DEGs with differential enrichment of various histone marks in leaf and root.

Figure S8. The role of histone marks in the induction of PEG-responsive genes.

Figure S9. Genome browser screen shots of histone mark enrichment in some common DEGs (identified in Figure 6) with 7 histone marks changing between leaf and root but not in response to PEG treatment.

Figure S10 Heat maps showing fold change (log2FC) of expression and histone marks of lignin biosynthesis genes

Table S1 Total reads and mapping rate of ChIP-seq data

Table S2 Changes of expression and histone marks of stress genes

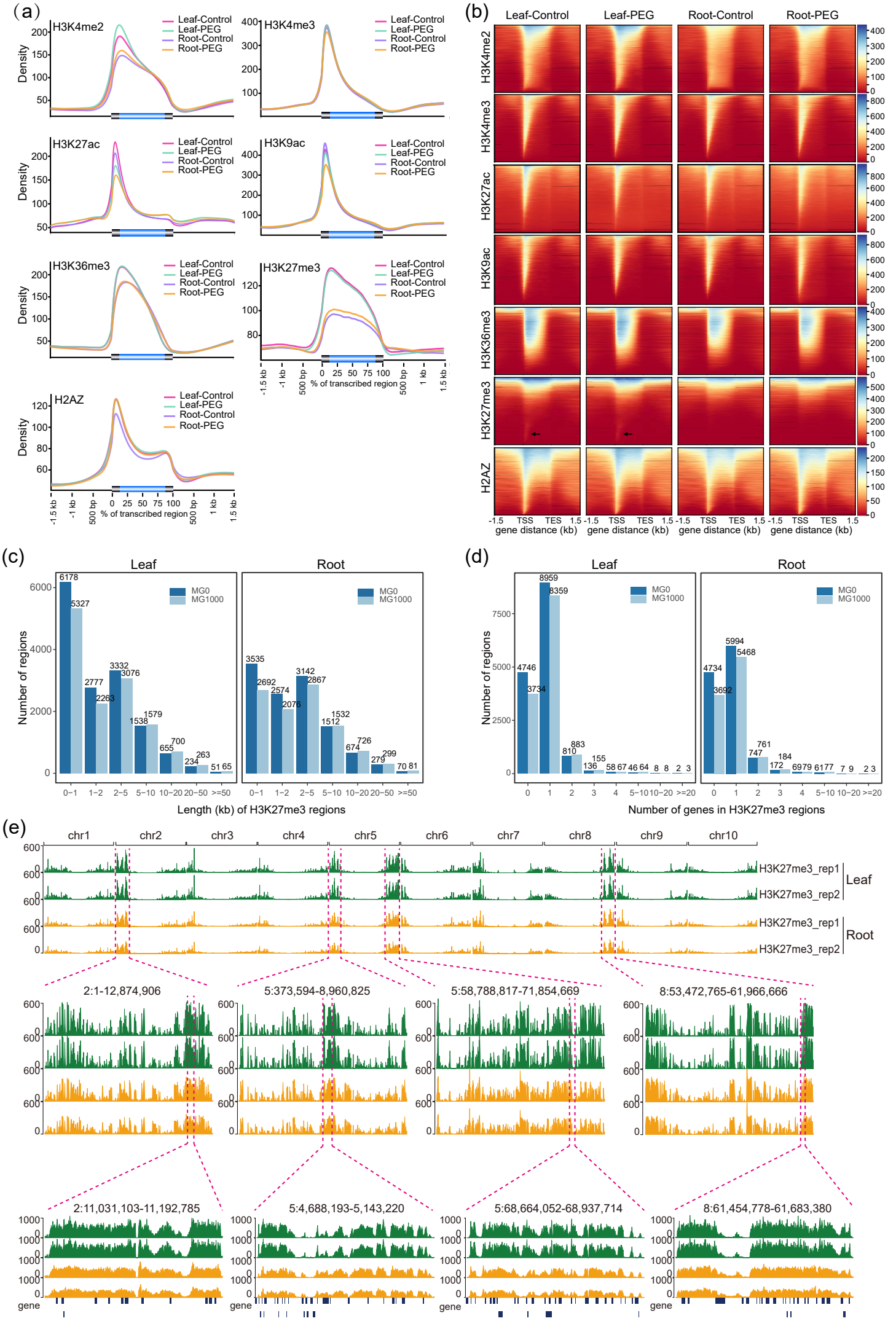
(a)
H3K4me2
H3K4me3
H3K27ac
H3K9ac
H3K36me3
H3K27me3
H2AZ
Leaf-Control
Leaf-PEG
Root-Control
Root-PEG
Density
% of transcribed region
(b)
Leaf-Control
Leaf-PEG
Root-Control
Root-PEG
gene distance (kb)
TSS
TES
(c)
Leaf
Root
MG0
MG1000
Number of regions
Length (kb) of H3K27me3 regions
(d)
Number of genes in H3K27me3 regions
(e)
chr1
chr2
chr3
chr4
chr5
chr6
chr7
chr8
chr9
chr10
H3K27me3_rep1
H3K27me3_rep2
Leaf
Root
2:1-12,874,906
5:373,594-8,960,825
5:58,788,817-71,854,669
8:53,472,765-61,966,666
2:11,031,103-11,192,785
5:4,688,193-5,143,220
5:68,664,052-68,937,714
8:61,454,778-61,683,380
gene

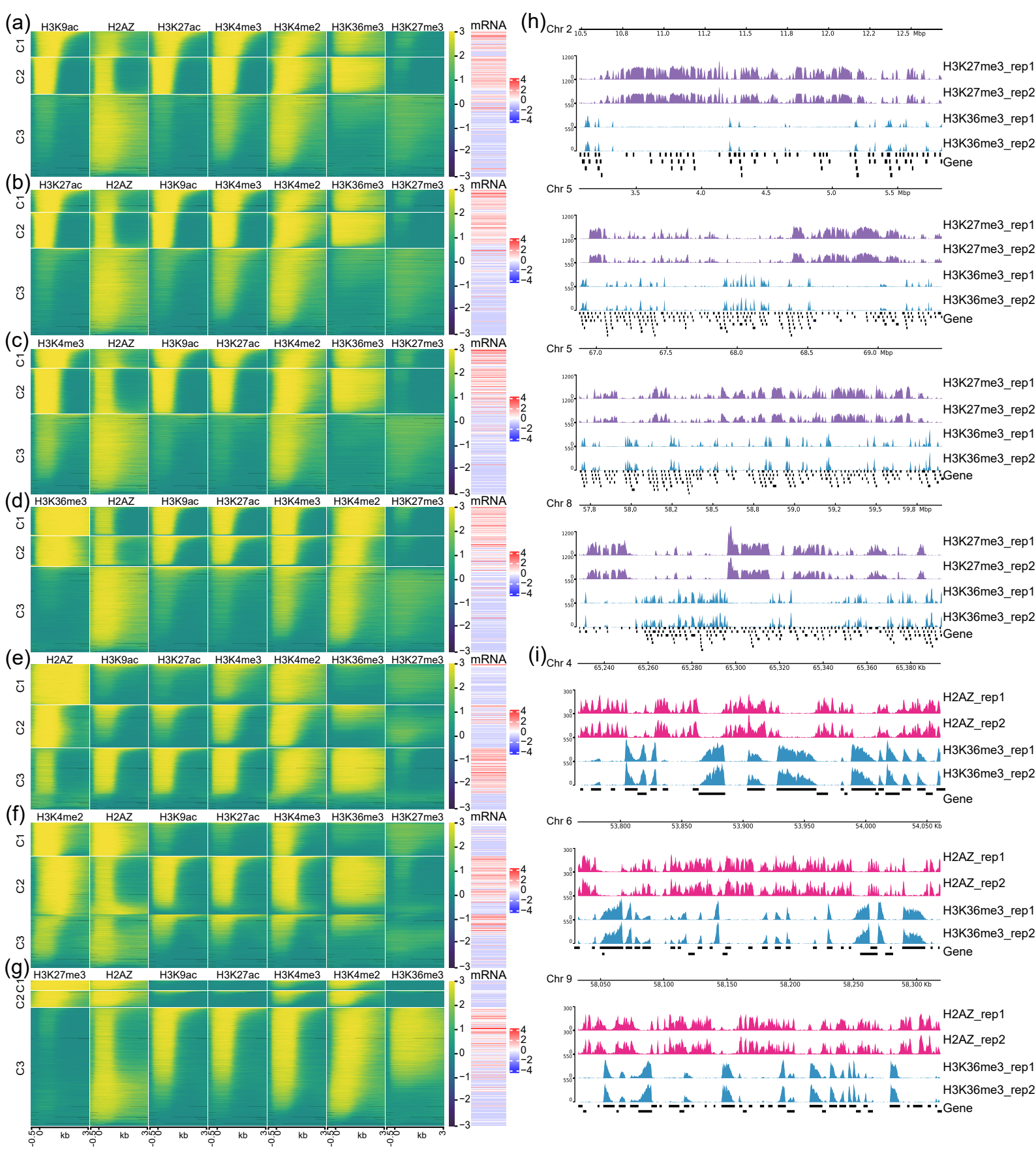
(a)
H3K9ac H2AZ H3K27ac H3K4me3 H3K4me2 H3K36me3 H3K27me3
mRNA
C1
C2
C3
(b)
H3K27ac H2AZ H3K9ac H3K4me3 H3K4me2 H3K36me3 H3K27me3
(c)
H3K4me3 H2AZ H3K9ac H3K27ac H3K4me2 H3K36me3 H3K27me3
(d)
H3K36me3 H2AZ H3K9ac H3K27ac H3K4me3 H3K4me2 H3K27me3
(e)
H2AZ H3K9ac H3K27ac H3K4me3 H3K4me2 H3K36me3 H3K27me3
(f)
H3K4me2 H2AZ H3K9ac H3K27ac H3K4me3 H3K36me3 H3K27me3
(g)
H3K27me3 H2AZ H3K9ac H3K27ac H3K4me3 H3K4me2 H3K36me3
kb
(h)
Chr 2
Chr 5
Chr 8
H3K27me3_rep1
H3K27me3_rep2
H3K36me3_rep1
H3K36me3_rep2
Gene
(i)
Chr 4
Chr 6
Chr 9
H2AZ_rep1
H2AZ_rep2
H3K36me3_rep1
H3K36me3_rep2
Gene

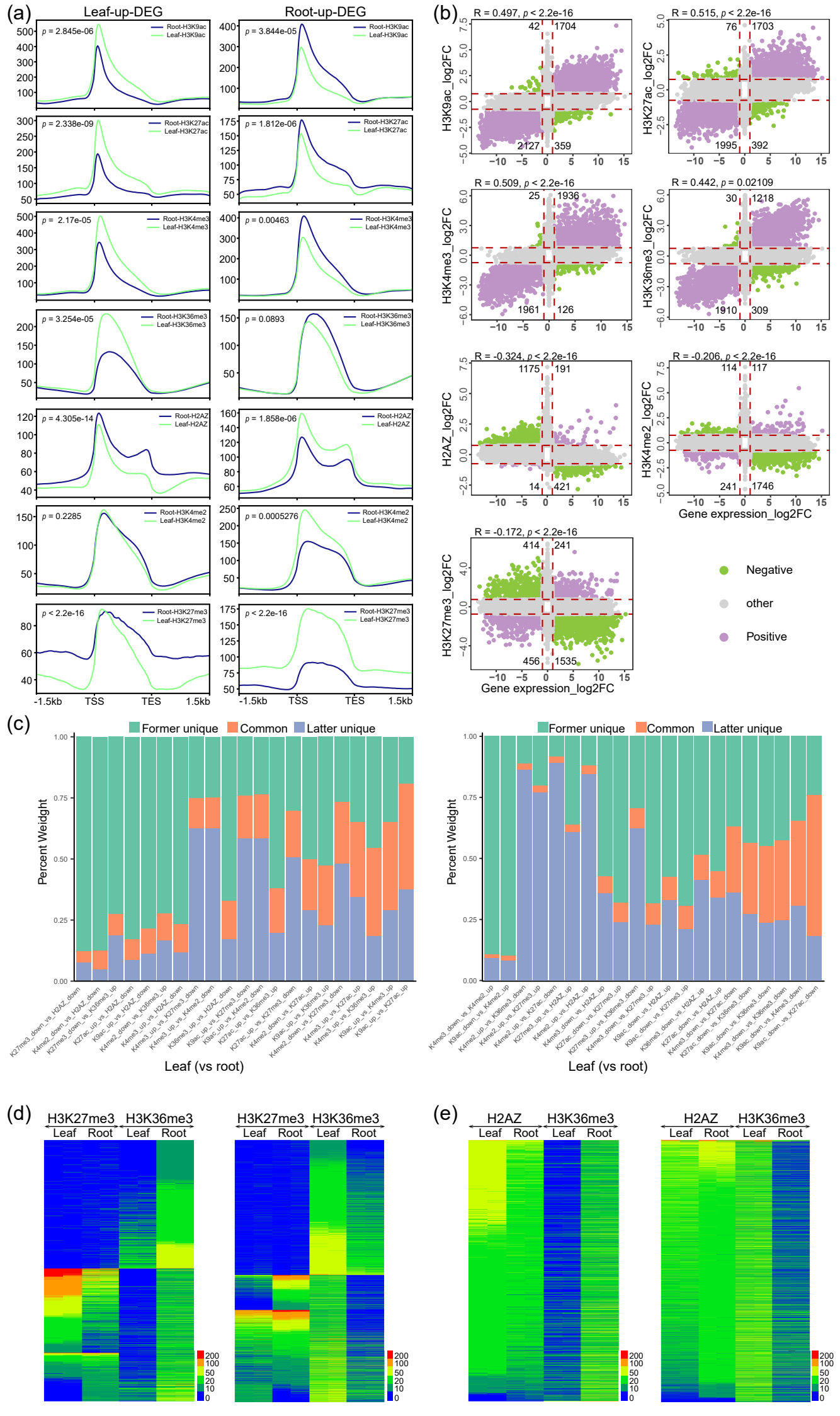
(a)
Leaf-up-DEG
Root-up-DEG
Root-H3K9ac
Leaf-H3K9ac
Root-H3K27ac
Leaf-H3K27ac
Root-H3K4me3
Leaf-H3K4me3
Root-H3K36me3
Leaf-H3K36me3
Root-H2AZ
Leaf-H2AZ
Root-H3K4me2
Leaf-H3K4me2
Root-H3K27me3
Leaf-H3K27me3
-1.5kb
TSS
TES
1.5kb
(b)
R = 0.497, p < 2.2e-16
R = 0.515, p < 2.2e-16
R = 0.509, p < 2.2e-16
R = 0.442, p = 0.02109
R = -0.324, p < 2.2e-16
R = -0.206, p < 2.2e-16
R = -0.172, p < 2.2e-16
H3K9ac_log2FC
H3K27ac_log2FC
H3K4me3_log2FC
H3K36me3_log2FC
H2AZ_log2FC
H3K4me2_log2FC
H3K27me3_log2FC
Gene expression_log2FC
Negative
other
Positive
(c)
Former unique
Common
Latter unique
Percent Weidght
Leaf (vs root)
(d)
H3K27me3
H3K36me3
Leaf
Root
(e)
H2AZ
H3K36me3
Leaf
Root

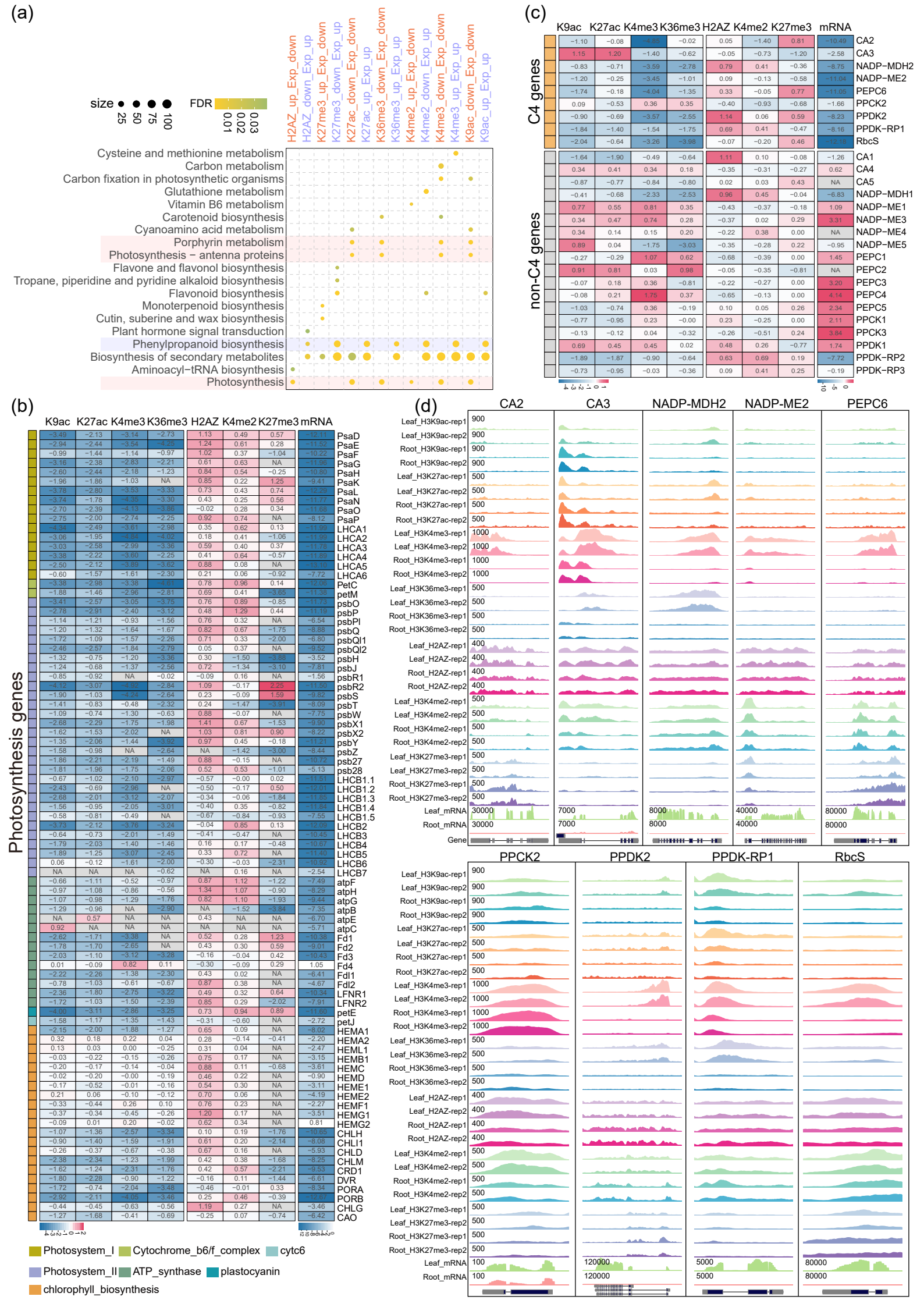
(a)
size
25
50
75
100
FDR
0.01
0.02
0.03
H2AZ_up_Exp_down
H2AZ_down_Exp_up
K27me3_up_Exp_down
K27me3_down_Exp_up
K27ac_down_Exp_down
K27ac_up_Exp_up
K36me3_down_Exp_down
K36me3_up_Exp_up
K4me2_up_Exp_down
K4me2_down_Exp_up
K4me3_down_Exp_down
K4me3_up_Exp_up
K9ac_down_Exp_down
K9ac_up_Exp_up
Cysteine and methionine metabolism
Carbon metabolism
Carbon fixation in photosynthetic organisms
Glutathione metabolism
Vitamin B6 metabolism
Carotenoid biosynthesis
Cyanoamino acid metabolism
Porphyrin metabolism
Photosynthesis − antenna proteins
Flavone and flavonol biosynthesis
Tropane, piperidine and pyridine alkaloid biosynthesis
Flavonoid biosynthesis
Monoterpenoid biosynthesis
Cutin, suberine and wax biosynthesis
Plant hormone signal transduction
Phenylpropanoid biosynthesis
Biosynthesis of secondary metabolites
Aminoacyl−tRNA biosynthesis
Photosynthesis
(b)
K9ac K27ac K4me3 K36me3 H2AZ K4me2 K27me3 mRNA
Photosynthesis genes
PsaD PsaE PsaF PsaG PsaH PsaK PsaL PsaN PsaO PsaP
LHCA1 LHCA2 LHCA3 LHCA4 LHCA5 LHCA6
PetC petM
psbO psbP psbPl psbQ psbQl1 psbQl2 psbH psbJ psbR1 psbR2 psbS psbT psbW psbX1 psbX2 psbY psbZ psb27 psb28
LHCB1.1 LHCB1.2 LHCB1.3 LHCB1.4 LHCB1.5 LHCB2 LHCB3 LHCB4 LHCB5 LHCB6 LHCB7
atpF atpH atpG atpB atpE atpC
Fd1 Fd2 Fd3 Fd4 Fdl1 Fdl2 LFNR1 LFNR2 petE petJ
HEMA1 HEMA2 HEML1 HEMB1 HEMC HEMD HEME1 HEME2 HEMF1 HEMG1 HEMG2
CHLH CHLI1 CHLD CHLM CRD1 DVR PORA PORB CHLG CAO
Photosystem_I
Cytochrome_b6/f_complex
cytc6
Photosystem_II
ATP_synthase
plastocyanin
chlorophyll_biosynthesis
(c)
K9ac K27ac K4me3 K36me3 H2AZ K4me2 K27me3 mRNA
C4 genes
CA2 CA3 NADP−MDH2 NADP−ME2 PEPC6 PPCK2 PPDK2 PPDK−RP1 RbcS
non-C4 genes
CA1 CA4 CA5 NADP−MDH1 NADP−ME1 NADP−ME3 NADP−ME4 NADP−ME5 PEPC1 PEPC2 PEPC3 PEPC4 PEPC5 PPCK1 PPCK3 PPDK1 PPDK−RP2 PPDK−RP3
(d)
CA2 CA3 NADP-MDH2 NADP-ME2 PEPC6
Leaf_H3K9ac-rep1
Leaf_H3K9ac-rep2
Root_H3K9ac-rep1
Root_H3K9ac-rep2
Leaf_H3K27ac-rep1
Leaf_H3K27ac-rep2
Root_H3K27ac-rep1
Root_H3K27ac-rep2
Leaf_H3K4me3-rep1
Leaf_H3K4me3-rep2
Root_H3K4me3-rep1
Root_H3K4me3-rep2
Leaf_H3K36me3-rep1
Leaf_H3K36me3-rep2
Root_H3K36me3-rep1
Root_H3K36me3-rep2
Leaf_H2AZ-rep1
Leaf_H2AZ-rep2
Root_H2AZ-rep1
Root_H2AZ-rep2
Leaf_H3K4me2-rep1
Leaf_H3K4me2-rep2
Root_H3K4me2-rep1
Root_H3K4me2-rep2
Leaf_H3K27me3-rep1
Leaf_H3K27me3-rep2
Root_H3K27me3-rep1
Root_H3K27me3-rep2
Leaf_mRNA
Root_mRNA
Gene
PPCK2 PPDK2 PPDK-RP1 RbcS

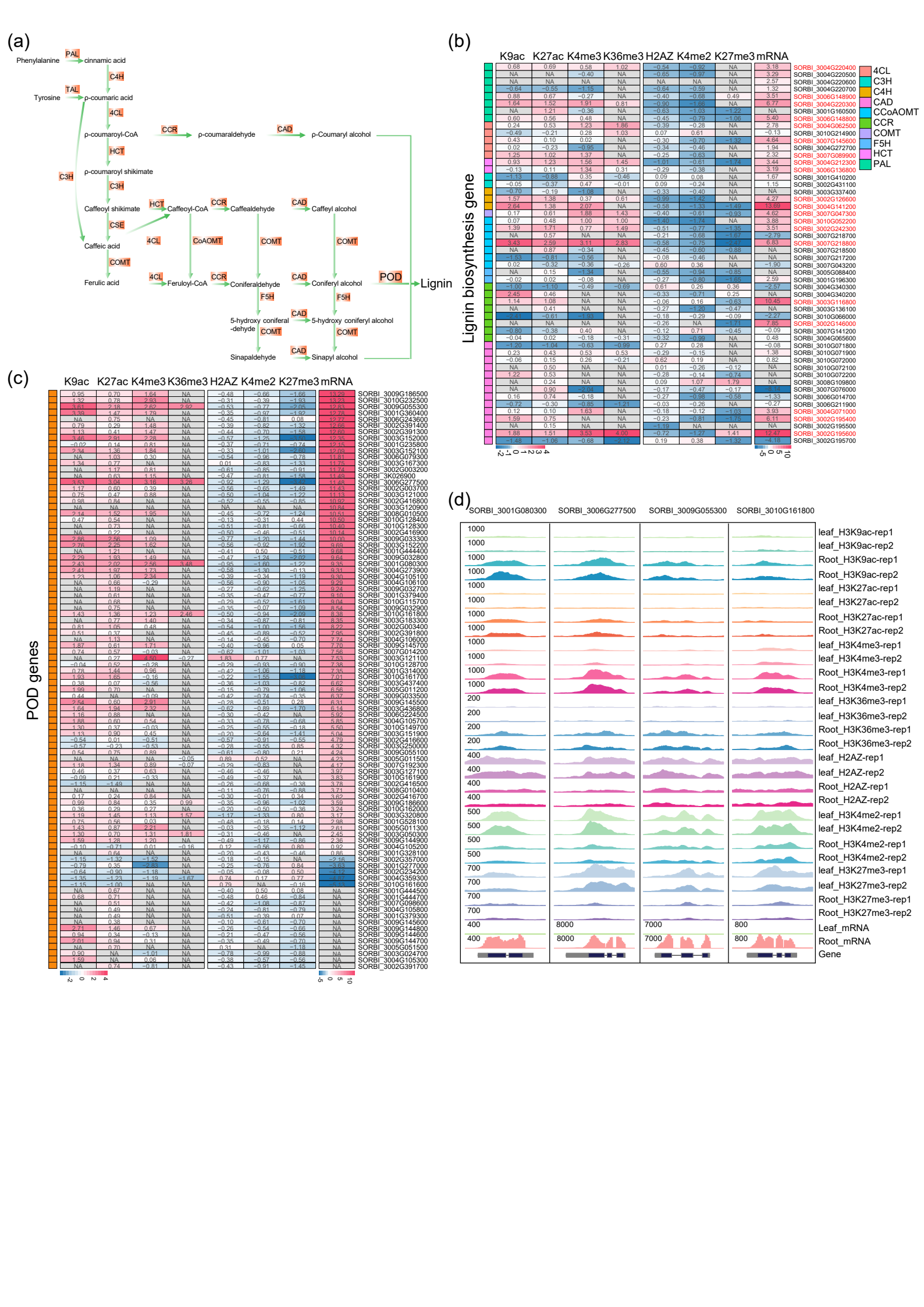
(a)
Phenylalanine
PAL
cinnamic acid
C4H
Tyrosine
TAL
p-coumaric acid
4CL
p-coumaroyl-CoA
CCR
p-coumaraldehyde
CAD
p-Coumaryl alcohol
HCT
p-coumaroyl shikimate
C3H
C3H
Caffeoyl shikimate
HCT
Caffeoyl-CoA
CCR
Caffealdehyde
CAD
Caffeyl alcohol
CSE
4CL
CoAOMT
COMT
COMT
Caffeic acid
COMT
Ferulic acid
4CL
Feruloyl-CoA
CCR
Coniferaldehyde
CAD
Coniferyl alcohol
POD
Lignin
F5H
F5H
CAD
5-hydroxy coniferal -dehyde
5-hydroxy coniferyl alcohol
COMT
COMT
CAD
Sinapaldehyde
Sinapyl alcohol
(b)
K9ac K27ac K4me3 K36me3 H2AZ K4me2 K27me3 mRNA
Lignin biosynthesis gene
4CL
C3H
C4H
CAD
CCoAOMT
CCR
COMT
F5H
HCT
PAL
(c)
K9ac K27ac K4me3 K36me3 H2AZ K4me2 K27me3 mRNA
POD genes
(d)
SORBI_3001G080300
SORBI_3006G277500
SORBI_3009G055300
SORBI_3010G161800
leaf_H3K9ac-rep1
leaf_H3K9ac-rep2
Root_H3K9ac-rep1
Root_H3K9ac-rep2
leaf_H3K27ac-rep1
leaf_H3K27ac-rep2
Root_H3K27ac-rep1
Root_H3K27ac-rep2
leaf_H3K4me3-rep1
leaf_H3K4me3-rep2
Root_H3K4me3-rep1
Root_H3K4me3-rep2
leaf_H3K36me3-rep1
leaf_H3K36me3-rep2
Root_H3K36me3-rep1
Root_H3K36me3-rep2
leaf_H2AZ-rep1
leaf_H2AZ-rep2
Root_H2AZ-rep1
Root_H2AZ-rep2
leaf_H3K4me2-rep1
leaf_H3K4me2-rep2
Root_H3K4me2-rep1
Root_H3K4me2-rep2
leaf_H3K27me3-rep1
leaf_H3K27me3-rep2
Root_H3K27me3-rep1
Root_H3K27me3-rep2
Leaf_mRNA
Root_mRNA
Gene

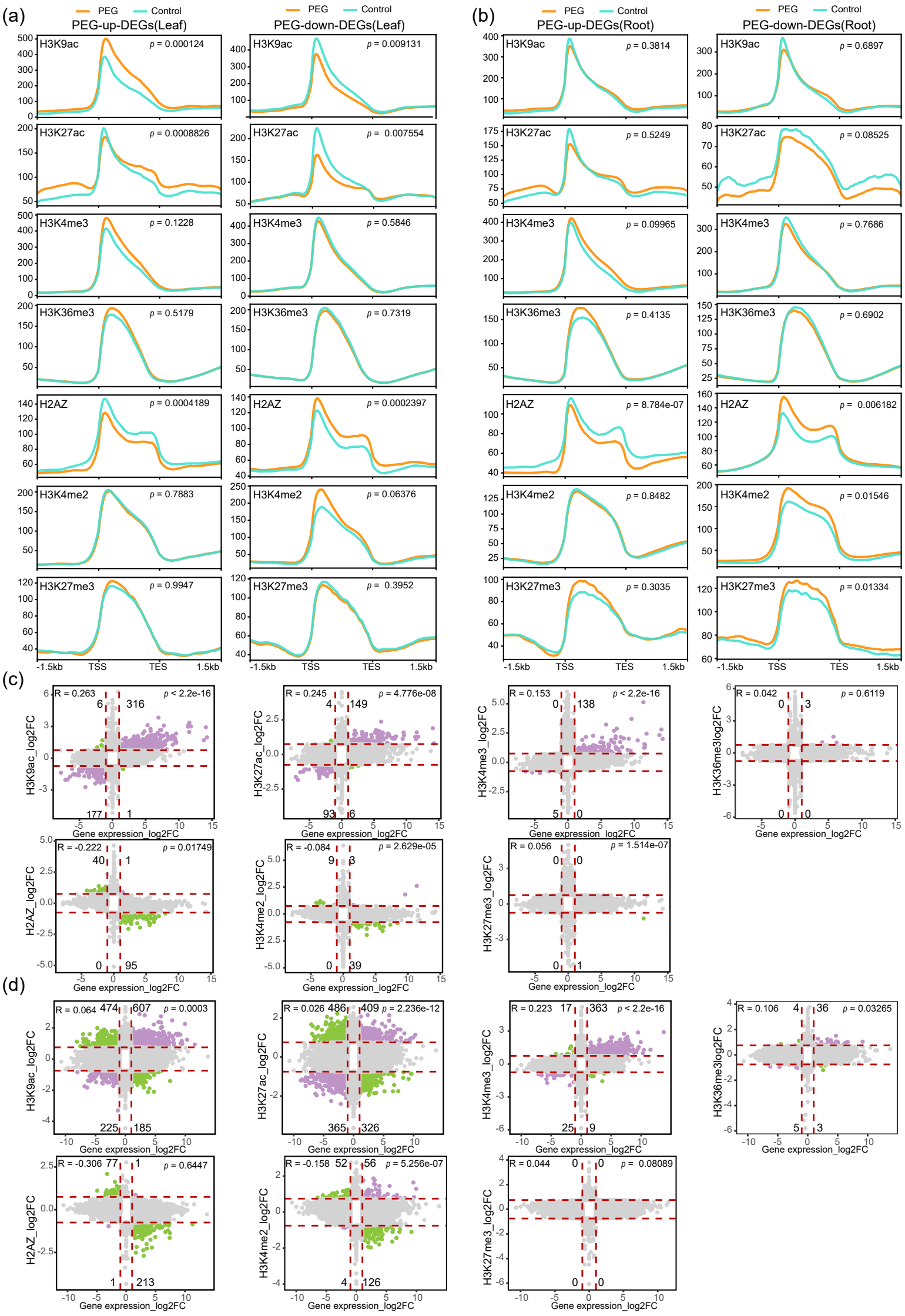
(a)
PEG
Control
PEG-up-DEGs(Leaf)
PEG-down-DEGs(Leaf)
H3K9ac
p = 0.000124
p = 0.009131
H3K27ac
p = 0.0008826
p = 0.007554
H3K4me3
p = 0.1228
p = 0.5846
H3K36me3
p = 0.5179
p = 0.7319
H2AZ
p = 0.0004189
p = 0.0002397
H3K4me2
p = 0.7883
p = 0.06376
H3K27me3
p = 0.9947
p = 0.3952
-1.5kb
TSS
TES
1.5kb
(b)
PEG-up-DEGs(Root)
PEG-down-DEGs(Root)
p = 0.3814
p = 0.6897
p = 0.5249
p = 0.08525
p = 0.09965
p = 0.7686
p = 0.4135
p = 0.6902
p = 8.784e-07
p = 0.006182
p = 0.8482
p = 0.01546
p = 0.3035
p = 0.01334
(c)
R = 0.263
p < 2.2e-16
6
316
177
1
H3K9ac_log2FC
Gene expression_log2FC
R = 0.245
p = 4.776e-08
4
149
93
6
H3K27ac_log2FC
R = 0.153
p < 2.2e-16
0
138
5
0
H3K4me3_log2FC
R = 0.042
p = 0.6119
0
3
0
0
H3K36me3log2FC
R = -0.222
p = 0.01749
40
1
0
95
H2AZ_log2FC
R = -0.084
p = 2.629e-05
9
3
0
39
H3K4me2_log2FC
R = 0.056
p = 1.514e-07
0
0
0
1
H3K27me3_log2FC
(d)
R = 0.064
474
607
p = 0.0003
225
185
H3K9ac_log2FC
Gene expression_log2FC
R = 0.026
486
409
p = 2.236e-12
365
326
H3K27ac_log2FC
R = 0.223
17
363
p < 2.2e-16
25
9
H3K4me3_log2FC
R = 0.106
4
36
p = 0.03265
5
3
H3K36me3log2FC
R = -0.306
77
1
p = 0.6447
1
213
H2AZ_log2FC
R = -0.158
52
56
p = 5.256e-07
4
126
H3K4me2_log2FC
R = 0.044
0
0
p = 0.08089
0
0
H3K27me3_log2FC

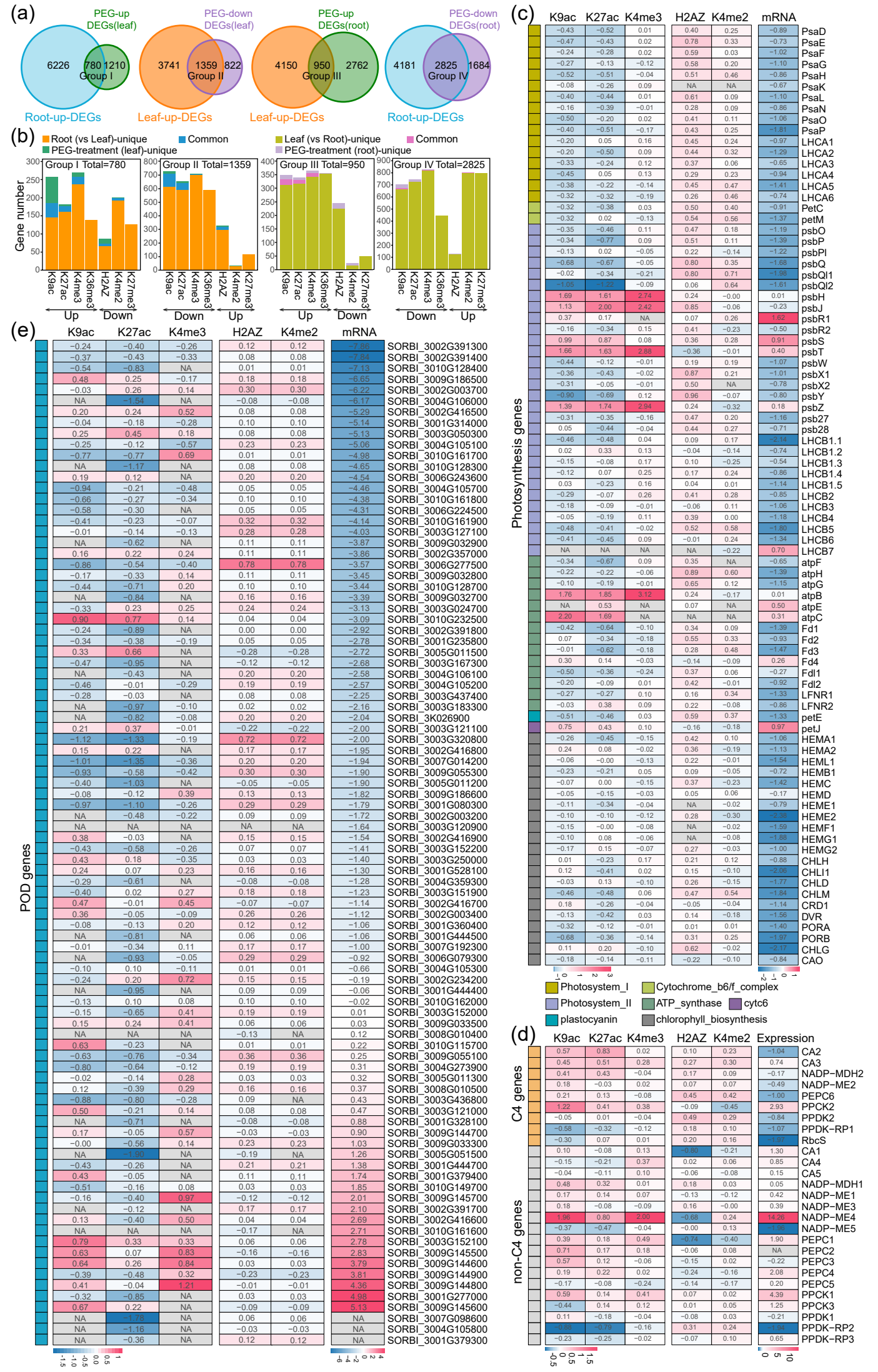
(a)
PEG-up DEGs(leaf)
PEG-down DEGs(leaf)
PEG-up DEGs(root)
PEG-down DEGs(root)
6226
780
1210
Group I
3741
1359
822
Group II
4150
950
2762
Group III
4181
2825
1684
Group IV
Root-up-DEGs
Leaf-up-DEGs
Leaf-up-DEGs
Root-up-DEGs
(b)
Root (vs Leaf)-unique
Common
Leaf (vs Root)-unique
Common
PEG-treatment (leaf)-unique
PEG-treatment (root)-unique
Gene number
Group I Total=780
Group II Total=1359
Group III Total=950
Group IV Total=2825
K9ac
K27ac
K4me3
K36me3
H2AZ
K4me2
K27me3
Up
Down
(c)
K9ac
K27ac
K4me3
H2AZ
K4me2
mRNA
Photosynthesis genes
PsaD
PsaE
PsaF
PsaG
PsaH
PsaK
PsaL
PsaN
PsaO
PsaP
LHCA1
LHCA2
LHCA3
LHCA4
LHCA5
LHCA6
PetC
petM
psbO
psbP
psbPl
psbQ
psbQl1
psbQl2
psbH
psbJ
psbR1
psbR2
psbS
psbT
psbW
psbX1
psbX2
psbY
psbZ
psb27
psb28
LHCB1.1
LHCB1.2
LHCB1.3
LHCB1.4
LHCB1.5
LHCB2
LHCB3
LHCB4
LHCB5
LHCB6
LHCB7
atpF
atpH
atpG
atpB
atpE
atpC
Fd1
Fd2
Fd3
Fd4
Fdl1
Fdl2
LFNR1
LFNR2
petE
petJ
HEMA1
HEMA2
HEML1
HEMB1
HEMC
HEMD
HEME1
HEME2
HEMF1
HEMG1
HEMG2
CHLH
CHLI1
CHLD
CHLM
CRD1
DVR
PORA
PORB
CHLG
CAO
Photosystem_I
Cytochrome_b6/f_complex
Photosystem_II
ATP_synthase
cytc6
plastocyanin
chlorophyll_biosynthesis
(d)
K9ac
K27ac
K4me3
H2AZ
K4me2
Expression
C4 genes
non-C4 genes
CA2
CA3
NADP−MDH2
NADP−ME2
PEPC6
PPCK2
PPDK2
PPDK−RP1
RbcS
CA1
CA4
CA5
NADP−MDH1
NADP−ME1
NADP−ME3
NADP−ME4
NADP−ME5
PEPC1
PEPC2
PEPC3
PEPC4
PEPC5
PPCK1
PPCK3
PPDK1
PPDK−RP2
PPDK−RP3
(e)
K9ac
K27ac
K4me3
H2AZ
K4me2
mRNA
POD genes
SORBI_3002G391300
SORBI_3002G391400
SORBI_3010G128400
SORBI_3009G186500
SORBI_3002G003700
SORBI_3004G106000
SORBI_3002G416500
SORBI_3001G314000
SORBI_3003G050300
SORBI_3004G105100
SORBI_3010G161700
SORBI_3010G128300
SORBI_3006G243600
SORBI_3004G105700
SORBI_3010G161800
SORBI_3006G224500
SORBI_3010G161900
SORBI_3003G127100
SORBI_3009G032900
SORBI_3002G357000
SORBI_3006G277500
SORBI_3009G032800
SORBI_3010G128700
SORBI_3009G032700
SORBI_3003G024700
SORBI_3010G232500
SORBI_3002G391800
SORBI_3001G235800
SORBI_3005G011500
SORBI_3003G167300
SORBI_3004G106100
SORBI_3004G105200
SORBI_3003G437400
SORBI_3003G183300
SORBI_3K026900
SORBI_3003G121100
SORBI_3003G320800
SORBI_3002G416800
SORBI_3007G014200
SORBI_3009G055300
SORBI_3005G011200
SORBI_3009G186600
SORBI_3001G080300
SORBI_3002G003200
SORBI_3003G120900
SORBI_3002G416900
SORBI_3003G152200
SORBI_3003G250000
SORBI_3001G528100
SORBI_3004G359300
SORBI_3003G151900
SORBI_3002G416700
SORBI_3002G003400
SORBI_3001G360400
SORBI_3001G444500
SORBI_3007G192300
SORBI_3006G079300
SORBI_3004G105300
SORBI_3002G234200
SORBI_3001G444400
SORBI_3010G162000
SORBI_3003G152000
SORBI_3009G033500
SORBI_3008G010400
SORBI_3010G115700
SORBI_3009G055100
SORBI_3004G273900
SORBI_3005G011300
SORBI_3008G010500
SORBI_3003G436800
SORBI_3003G121000
SORBI_3001G328100
SORBI_3009G144700
SORBI_3009G033300
SORBI_3005G051500
SORBI_3001G444700
SORBI_3001G379400
SORBI_3010G149700
SORBI_3009G145700
SORBI_3002G391700
SORBI_3002G416600
SORBI_3010G161600
SORBI_3003G152100
SORBI_3009G145500
SORBI_3009G144600
SORBI_3009G144900
SORBI_3009G144800
SORBI_3001G277000
SORBI_3009G145600
SORBI_3007G098600
SORBI_3004G105800
SORBI_3001G379300

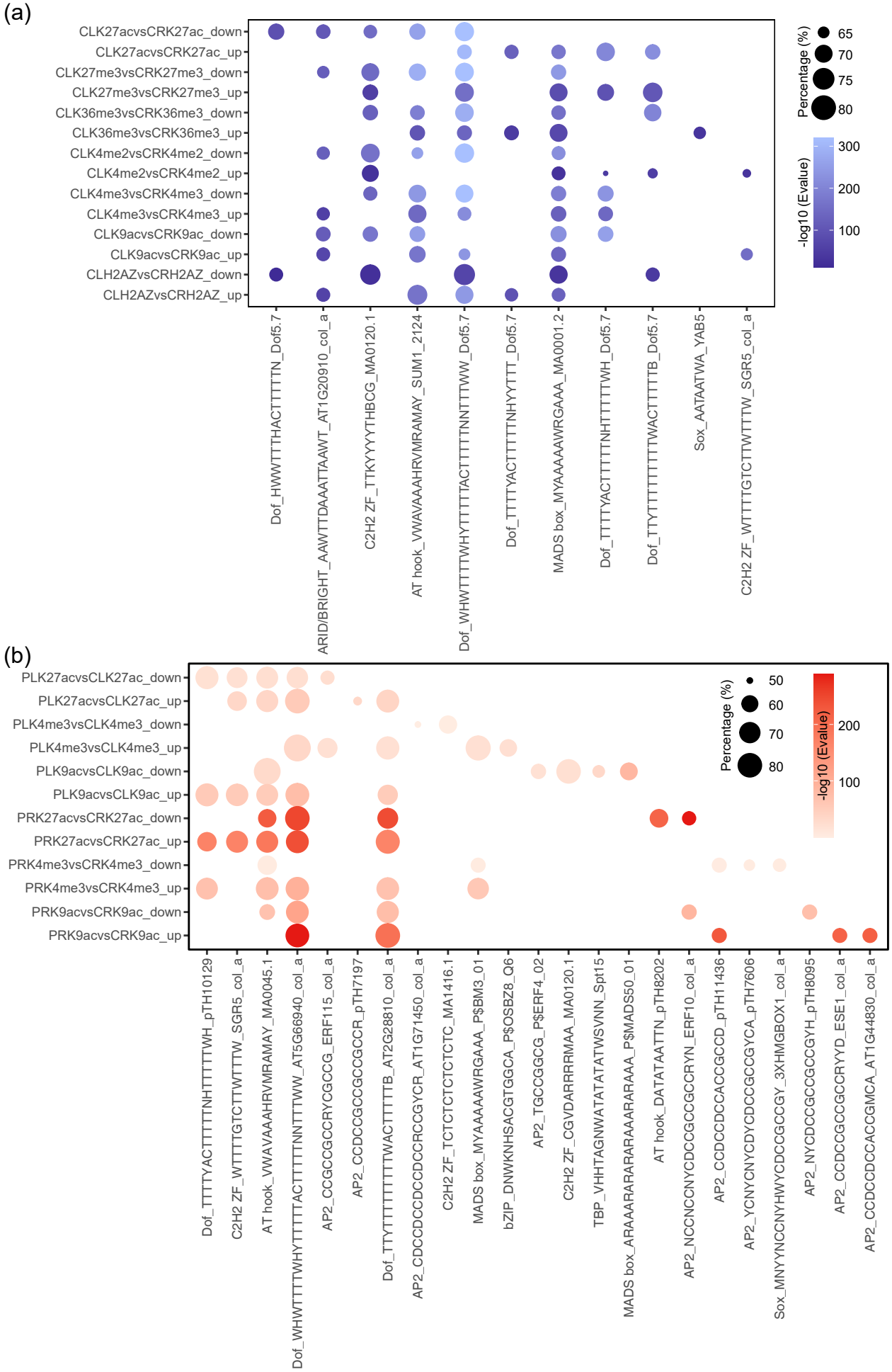
(a)
CLK27acvsCRK27ac_down
CLK27acvsCRK27ac_up
CLK27me3vsCRK27me3_down
CLK27me3vsCRK27me3_up
CLK36me3vsCRK36me3_down
CLK36me3vsCRK36me3_up
CLK4me2vsCRK4me2_down
CLK4me2vsCRK4me2_up
CLK4me3vsCRK4me3_down
CLK4me3vsCRK4me3_up
CLK9acvsCRK9ac_down
CLK9acvsCRK9ac_up
CLH2AZvsCRH2AZ_down
CLH2AZvsCRH2AZ_up
Dof_HWWTTTHACTTTTTN_Dof5.7
ARID/BRIGHT_AAWTTDAAATTAAWT_AT1G20910_col_a
C2H2 ZF_TTKYYYYTHBCG_MA0120.1
AT hook_VWAVAAAHRVMRAMAY_SUM1_2124
Dof_WHWTTTTWHYTTTTTACTTTTTNNTTTWW_Dof5.7
Dof_TTTTTYACTTTTTNHYYTTT_Dof5.7
MADS box_MYAAAAAWRGAAA_MA0001.2
Dof_TTTTTYACTTTTTNHTTTTTWH_Dof5.7
Dof_TTYTTTTTTTTTTWACTTTTTB_Dof5.7
Sox_AATAATWA_YAB5
C2H2 ZF_WTTTTGTCTTWTTTW_SGR5_col_a
Percentage (%)
65
70
75
80
-log10 (Evalue)
300
200
100
(b)
PLK27acvsCLK27ac_down
PLK27acvsCLK27ac_up
PLK4me3vsCLK4me3_down
PLK4me3vsCLK4me3_up
PLK9acvsCLK9ac_down
PLK9acvsCLK9ac_up
PRK27acvsCRK27ac_down
PRK27acvsCRK27ac_up
PRK4me3vsCRK4me3_down
PRK4me3vsCRK4me3_up
PRK9acvsCRK9ac_down
PRK9acvsCRK9ac_up
Dof_TTTTYACTTTTTNHTTTTTWH_pTH10129
C2H2 ZF_WTTTTGTCTTWTTTW_SGR5_col_a
AT hook_VWAVAAAHRVMRAMAY_MA0045.1
Dof_WHWTTTTWHYTTTTTACTTTTTNNTTTWW_AT5G66940_col_a
AP2_CCGCCGCCRYCGCCG_ERF115_col_a
AP2_CCDCCGCCGCCGCCR_pTH7197
Dof_TTYTTTTTTTTTTWACTTTTTB_AT2G28810_col_a
AP2_CDCCDCCDCCDCCRCCGYCR_AT1G71450_col_a
C2H2 ZF_TCTCTCTCTCTCTC_MA1416.1
MADS box_MYAAAAAWRGAAA_P$BM3_01
bZIP_DNWKNHSACGTGGCA_P$OSBZ8_Q6
AP2_TGCCGGCG_P$ERF4_02
C2H2 ZF_CGVDARRRRMAA_MA0120.1
TBP_VHHTAGNWATATATATWSVNN_Spt15
MADS box_ARAAARARARARAAARAAAA_P$MADS50_01
AT hook_DATATAATTN_pTH8202
AP2_NCCNCCNYCDCCGCCGCCRYN_ERF10_col_a
AP2_CCDCCDCCACCGCCD_pTH11436
AP2_YCNYCNYCDYCDCCGCCGYCA_pTH7606
Sox_MNYYNCCNYHWYCDCCGCCGY_3XHMGBOX1_col_a
AP2_NYCDCCGCCGCCGYH_pTH8095
AP2_CCDCCGCCGCCRYYD_ESE1_col_a
AP2_CCDCCDCCACCGMCA_AT1G44830_col_a
Percentage (%)
50
60
70
80
-log10 (Evalue)
200
100